ELSEVIER

Chiral porous coordination networks: rational design and applications in enantioselective processes

Banu Kesanli, Wenbin Lin*

Department of Chemistry, CB#3290, University of North Carolina, Chapel Hill, NC 27599, USA

Contents

Abstract

This paper provides a short review of recent progress in the synthesis and characterization of homochiral metal-organic coordination networks (MOCNs) and their applications in the areas of asymmetric catalysis and chiral separations. Although chiral MOCNs can be constructed from achiral components, the resulting bulk solids tend to be racemic and are thus not useful for enantioselective processes. A couple of examples of homochiral solids built from achiral bridging ligands are presented along with more prevalent homochiral MOCNs built from chiral bridging ligands that are categorized based on their network dimensionality. Preliminary applications of these homochiral solids in asymmetric catalysis and chiral separations are also presented.
© 2003 Elsevier B.V. All rights reserved.

1. Introduction

Zeolites, a class of aluminosilicates with interconnected small cavities of 4–13 Å in dimensions, are used for the production of many consumer products ranging from gasoline to detergents and contribute to almost a trillion dollars of global economy annually [1]. For example, size-selective heterogeneous catalytic transformation of petrochemicals has been extensively used to improve the quality of gasoline, and thus significantly reduce the pollution from incomplete combustions of fossil fuels [2].

The presence of cations inside the channels and cavities of zeolites also make them ideal choices for ion exchange processes.

In light of the importance of chirality in biological processes, there have been tremendous research efforts devoted to the development of chiral zeolites and related porous solids over the past few decades. Although there have been breakthroughs in the synthesis of zeolites with larger pores, no chiral zeolites are available in enantipure form to date. Zeolite β and titanosilicate ETS-10 are the only two zeotypes that exist in chiral forms [3,4]. Zeolite β is a three-dimensional 12-ring pore system that can crystallize in a chiral polymorph, which is interconnected in either a left or right handed system. It is, however, extremely difficult (if not impossible) to obtain Zeolite β in enantipure

* Corresponding author. Tel.: +1-919-962-6320;
fax: +1-919-962-2388.
  E-mail address: wlin@unc.edu (W. Lin).

form. Likewise, it is also very difficult to obtain ETS-10 in enantiopure form [4]. The lack of chiral zeolites is in fact not surprising at all! Zeolites are typically synthesized in the presence of surfactant templates, which are removed through calcinations at 400–550 °C [5]. Attempts to synthesize chiral zeolites have uniformly relied on chiral surfactants to organize silicate-surfactant assemblies into chiral conformations. Unfortunately, calcinations at high temperatures invariably destroy the chiral conformation of such assemblies to result in either achiral or racemic mixtures of zeolites. New strategies are thus needed to prepare chiral zeolitic materials that may find practical applications in chirotechnology.

There has been a recent surge of research interest in metal-organic coordination networks (MOCNs) owing to their potential applications in catalysis, photonics, separation, gas storage, molecular sensing, and even drug delivery [6]. Compared to traditional zeolites and recently developed MCM-type mesoporous materials, MOCNs are synthesized under mild conditions and allow systematic engineering of chemical and physical properties through modifications of their components. Seminal work by Yaghi et al. has clearly established the feasibility of designing porous solids with controlled pore size and chemical functionality [7]. For example, reactions of the rigid linear organic linkers, 1,4-benzenedicarboxylate (BDC) groups with Zn(II) ions led to a series of isoreticular 3D porous MOCNs of general formula $Zn_4O(R\text{-}BDC)$ (denoted as IRMOF). Sixteen IRMOFs were prepared and all exhibited the same network topology (Scheme 1). The structure is made up of oxo-centered Zn_4O tetrahedron residing at the edges of the cube and bridged by six carboxylate units to give octahedron-shaped

secondary building units (SBUs). These SBUs are further linked by the bridging dicarboxylate groups to form the 3D cubic networks (Fig. 1). The pore size can be controlled by using carboxylate linkers of varying lengths such as biphenyl, tetrahydropyrene, pyrene, and terphenyl moieties. Additionally, various functional groups such as –Br, –NH_2, –OC_3H_7, –OC_5H_{11}, –C_2H_4 and –C_4H_4 were incorporated into the frameworks that are orientated towards the pores. The resulting networks are highly porous with very low crystal densities (Fig. 1). The void space for these network structures ranges from 55.8 to 91.1% of the total volume and the density is in the range of 1.0–0.21 g/cm^3. These materials have shown promise for applications in gas storage. For example, IRMOF-6 has a very high surface area of 2630 m^2/g and pore volume of 0.6 cm^3, and its methane storage capacity was measured to be 240 cm^3 at STP.

Although numerous examples of porous MOCNs have been reported in recent years, chiral porous MOCNs are still rare. Most chiral MOCNs reported to date were synthesized from achiral components [6c]. The chirality of these MOCNs originates from the spatial disposition of their building blocks and is not amenable to fine-tuning [6c]. Moreover, the bulk materials tend to be racemic even though single crystals are chiral. A straightforward approach is to construct chiral porous MOCNs using metal ions or metal clusters as nodes and chiral multifunctional ligands as linkers. In ideal scenarios, chiral pockets and/or functional groups reside inside the MOCNs, which can then be used for enantioselective separation and catalytic processes. Recent advances in the synthesis, characterization, and applications of homochiral MOCNs are reviewed in this article.
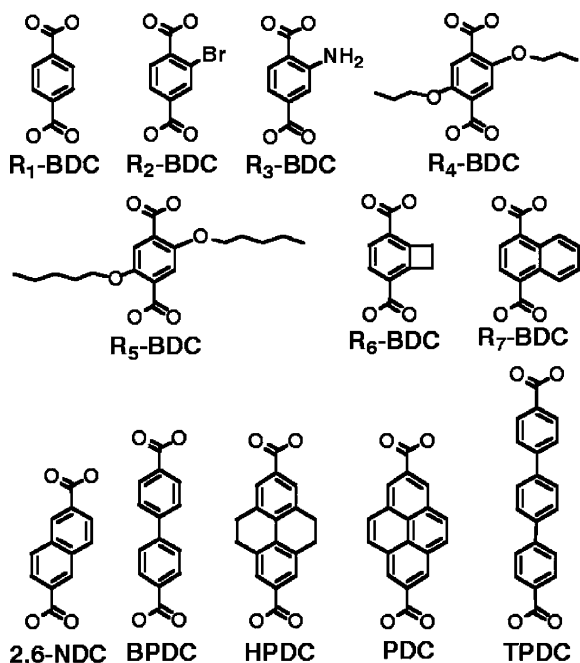
2. Homochiral MOCNs built from achiral bridging ligands

Chiral MOCNs can be synthesized from achiral components. Although individual crystals of such MOCNs can be chiral, their bulk samples tend to be racemic. Aoyama and coworkers recently reported an interesting example of homochiral crystallization of MOCNs that are built from achiral components [8]. When an achiral anthracene-pyrimidine derivative 5-(9-anthracenyl)pyrimidine, **L1**, was treated with $Cd(NO_3)_2\cdot4H_2O$, a helical coordination polymer with the composition of $Cd(\mathbf{L1})(NO_3)_2(H_2O)(EtOH)$, **1**, was obtained (Scheme 2). The Cd^{2+} center in **1** adopts octahedral geometry by coordinating to two pyrimidines, one water, one ethanol, and two nitrates. The twisting nature of the two coordinating pyrimidine rings on each Cd^{2+} center leads to the formation of a helical array of Cd^{2+}-pyrimidine coordination polymer which crystallizes in the chiral space group $P2_1$ (Fig. 2). Unlike the majority of chiral MOCNs made of achiral components, **1** possesses two unique features. First, adjacent helices adopt the same handedness and are linked by the interstrand H_2O-nitrate hydrogen-bonding

R_1-BDC R_2-BDC R_3-BDC R_4-BDC

R_5-BDC R_6-BDC R_7-BDC
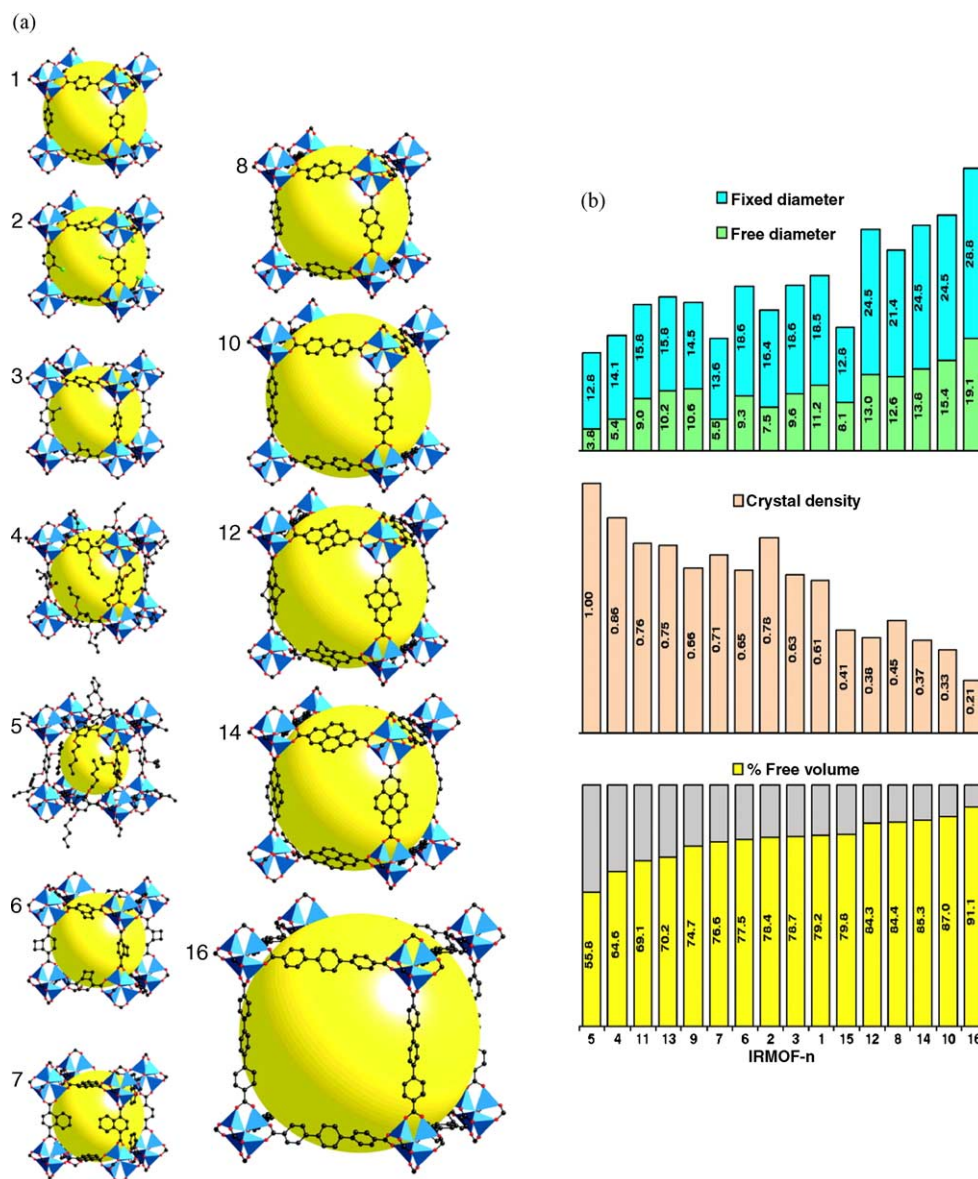
2,6-NDC   BPDC   HPDC   PDC   TPDC

Scheme 1.

Fig. 1. (a) Single crystal structures of IRMOF-*n* (*n* = 1–7, 8, 10, 12, 14, and 16). Coloring scheme: Zn (blue polyhedra), O (red), C (grey). (b) Bottom to top, the calculated percent free volume (yellow), crystal densities (light brown), and free diameter (green) and fixed diameter (blue), respectively, for IRMOF-1–16.

interactions. Such H-bonding interactions stabilize the helical structure and also ensure the attainment of chiral crystals of **1**. Second, the entire bulk sample of **1** is homochiral. Such homochirality was ascertained by solid-state circular

dichroism (CD) experiments and was explained in terms of the crystal growth mechanism. It is suggested that crystals grow as a single colony from the first formed nucleus, therefore, the stereochemistry of the first grown nucleus dictates
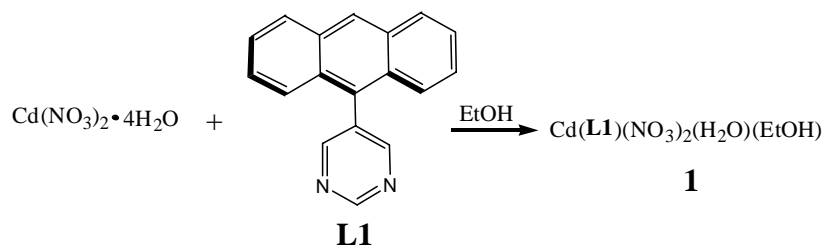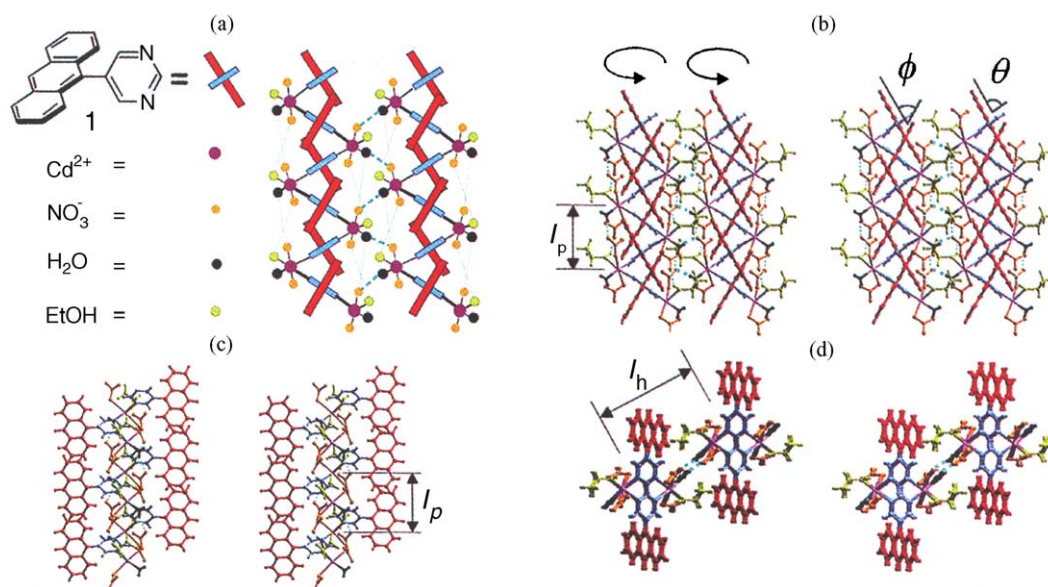

Scheme 2.

Fig. 2. Different views of the helical coordination network of Cd(**L1**)(NO$_3$)$_2$·H$_2$O·EtOH, **1**. (a) Schematic explanation of the front view; (b) front view; (c) side view of a helix chain and (d) top view of two neighboring helices H-bonded to form a sheet.

the stereochemistry of all the crystals. Aoyama et al. further demonstrated that the seeding technique could be used to grow crystals of desired stereochemistry. Seeding with M- or P-enantiomer resulted in the formation of enantiopure M- or P-crystals, respectively.

Metal 1,3,5-benzenetricarboxylate of the type M$_3$(btc)$_2$ is known to adopt an intrinsically chiral (10,3)-a network structure. However, bulk samples are achiral because of the presence of helices of both handedness in an achiral single crystal or equal probability for the formation of chiral crystals of both handedness. Rosseinsky et al. recently demonstrated the utility of coordinating chiral diols in directing the formation of homochiral porous networks of the type M$_3$(btc)$_2$ [9]. Based on the observation that diols can coordinate to the metal centers in a bidentate fashion to lead to MOCNs with reduced number of interpenetrated (10,3)-a nets, enantiomerically pure 1,2-propanediol (1,2-pd) was used to obtain doubly interpenetrated (10,3)-a network, Ni$_3$(btc)$_2$(py)$_6$(1,2-pd)$_3$·11(1,2-pd)·8(H$_2$O), **2**. In **2**, the coordinating 1,2-pd acts as a chiral template that controls not only the handedness of the helices but all the crystals to give rise to homochiral networks with chiral pores and cavities (Fig. 3). The equatorial positions of the octahedral Ni^{2+} centers are occupied by two pyridines and one bidentate 1,2-propanediol, while the axial positions are occupied by monodentate carboxylate groups of the btc ligands. Interestingly, X-ray and chiral GC studies indicated the *S*-enantiomer of 1,2-pd preferentially binds to the Ni center even when racemic 1,2-pd is used (with an enantio excess of ~20%). The framework of **2** is porous with a pore volume of 51% and channel size in the 10.5–16 Å range. The solvent molecules in **2** can be carefully removed below 145 °C to afford crystalline samples with both empty chiral pores and vacant coordination sites around the metal centers.

3. Homochiral MOCNs built from chiral bridging ligands

The most reliable strategy in designing homochiral MOCNs is to combine metal-containing nodes and chiral organic bridging ligands. The use of chiral bridging ligands will ensure the chirality in the resulting network structures. Various chiral bridging ligands have been utilized to construct chiral MOCNs, and this section will categorize chiral MOCNs based on their network dimensionality.

3.1. 1D homochiral MOCNs

Hosseini and coworkers designed a chiral tecton to coordinate with metal centers to generate a chiral and directional 1D network [10]. The ligand (**L2**) consists of a pyridine group on one end and a C$_2$-symmetric 2,6-bis(oxazolyl)-pyridine on the other end, and is thus chiral owing to the use of optically active oxazoline groups (Scheme 3). Slow diffusion of EtOH solutions of Co(II) ions into CHCl$_3$ solutions of **L2** afforded single crystals of neutral, 1D network structure with the formula of Co(**L2**)Cl$_2$·3CH$_3$CN, **3** (Fig. 4). Two different **L2** ligands occupy the equatorial positions through binding N atoms in a tridentate and monodentate fashion, respectively. The octahedral coordination around the Co^{2+} center in **3** is satisfied by two Cl$^-$ anions in axial positions. As the ligand is unsymmetrical and chiral, the 1D chains are chiral as well. These 1D chains adopt parallel packing in the solid to achieve a noncentrosymmetric arrangement of the dipoles of the 1D chains. The molecular chirality is thus successfully used to align molecular dipoles to lead to a polar solid.

Lin and coworkers has designed a variety of chiral bridging ligands based on atropisomeric 1,1′-binaphthyl frame-
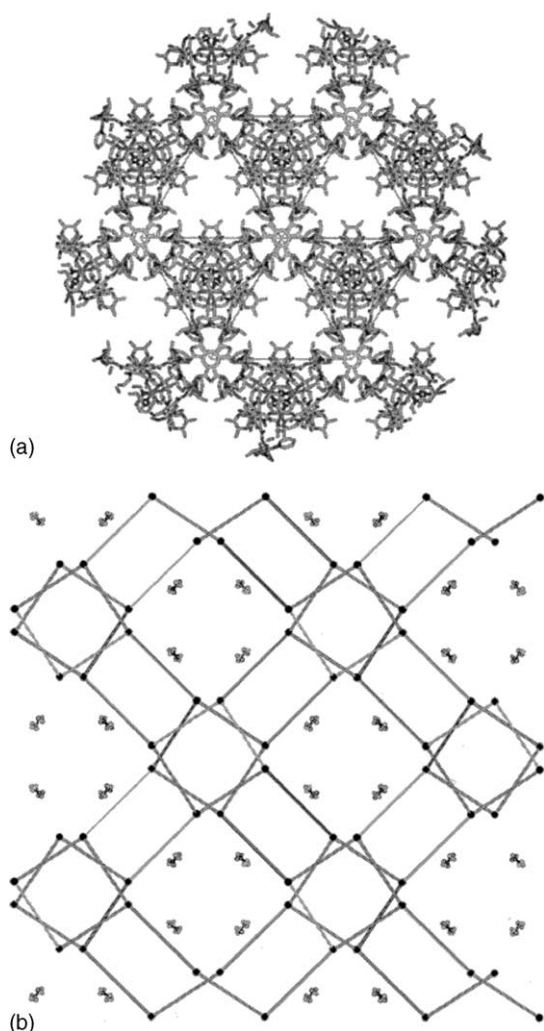
(a)

(b)

Fig. 3. Structure of $Ni_3(btc)_2(py)_6(1,2-pd)_3 \cdot 11(1,2-pd) \cdot 8(H_2O)$. (a) Showing different pore sizes and (b) containing 1,2-propandiol molecules.

work. When a linear metal connector $Ni(acac)_2$ (where acac is acetylacetonate) was combined with an axially chiral bridging organic ligand, 2,2′dimethoxy-1,1′-binaphthyl-3,3′-bis-(4-vinylpyridine) (**L3**), a 1D helical chain of [$Ni(acac)_2(L3)$], **4**, was obtained [11]. The **L3** ligand coordinates to the octahedral Ni^{2+} center in **4** through the N atom

L2
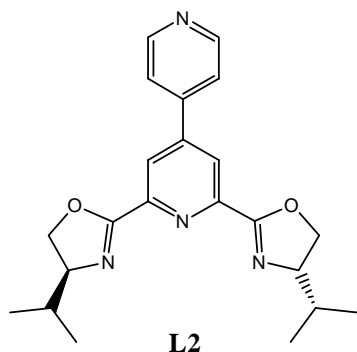
Scheme 3.
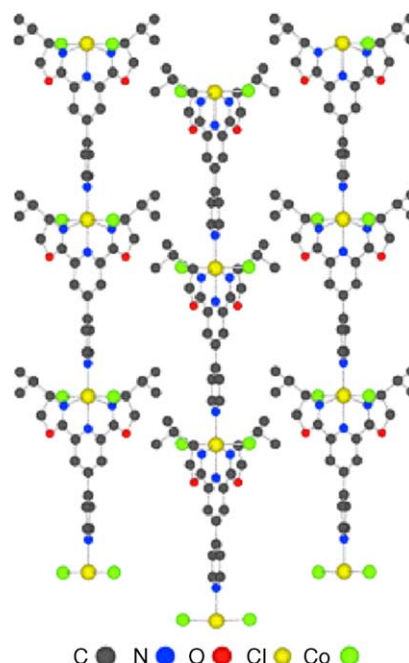
Fig. 4. 1D chiral network built from Co(II) and a chiral tecton **L2**.

of the pyridyl groups in *trans* positions, while the two bidentate acac units are in the equatorial positions. Infinite helical chain forms along the *b*-axis via linking adjacent $Ni(acac)_2$ groups with the binaphthyl backbone of the **L3** ligand. A single crystal X-ray diffraction study further showed that helical strands intertwine one another via van der Waals interactions to form a homochiral triple helix (Fig. 5). The π–π stacking interactions between the intertwined vinylnaphthyl groups of **L3** from adjacent triple helices direct the self-assembly of neighboring helices into 2D network in the *bc* plane that has a staggered arrangement. MeOH and H_2O solvent molecules fill the void space inside the homochiral solid.

Chiral bridging ligands with twisted dicarboxylate groups have also been used by Lin and coworkers to construct homochiral 1D MOCNs [12,13]. When enantiopure 2,2′-dihydroxy-1,1′-binaphthylene-6,6′-dicarboxylic acid (**L4**) was treated with various metal salts under slightly basic conditions, 1D homochiral MOCNs **5**–**9** with interesting topologies were obtained (Scheme 4).
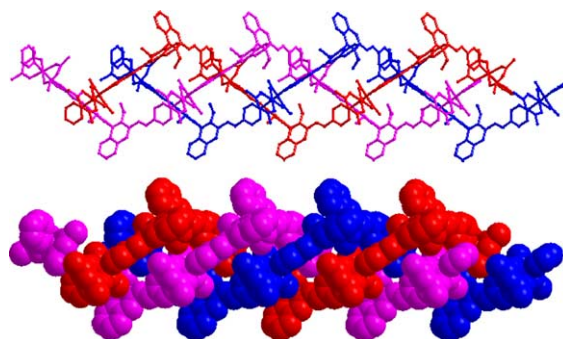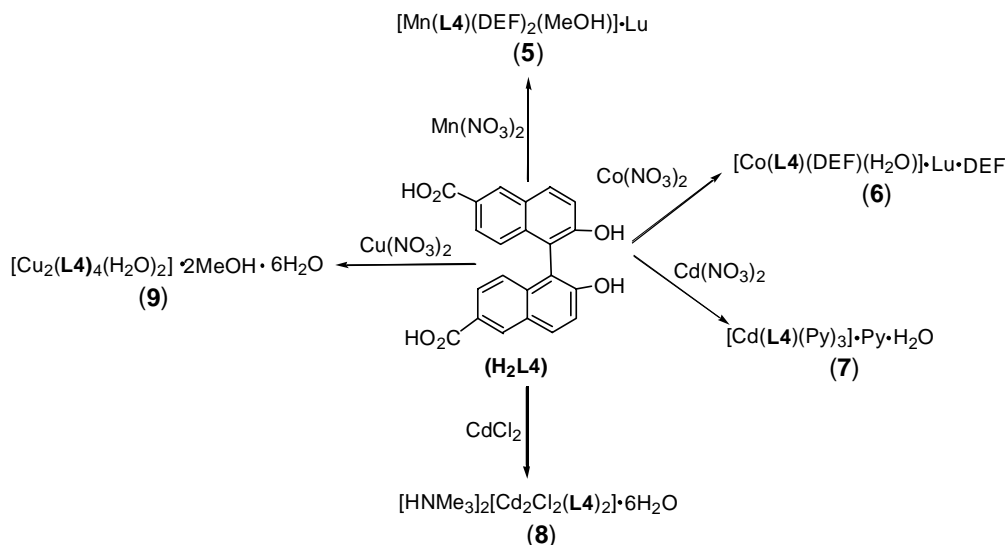

Fig. 5. Triple helix structure of [$Ni(acac)_2(L3)$], **4**.

[Mn(**L4**)(DEF)$_2$(MeOH)]·Lu
(5)

Mn(NO$_3$)$_2$

[Co(**L4**)(DEF)(H$_2$O)]·Lu·DEF
(6)

Co(NO$_3$)$_2$

HO$_2$C

OH

Cu(NO$_3$)$_2$

[Cu$_2$(**L4**)$_4$(H$_2$O)$_2$] ·2MeOH · 6H$_2$O
(9)

OH

Cd(NO$_3$)$_2$

HO$_2$C

(H$_2$L4)

[Cd(**L4**)(Py)$_3$]·Py·H$_2$O
(7)

CdCl$_2$

[HNMe$_3$]$_2$[Cd$_2$Cl$_2$(**L4**)$_2$]·6H$_2$O
(8)

Scheme 4.

In all the five complexes, the **L4** bridging ligands link adjacent metal centers to form 1D coordination polymeric chains using the carboxylate functionality (Fig. 6). The hydroxyl groups in the **L4** ligands then form H-bonds with carboxylate oxygen atoms to link 1D coordination polymeric chains into open frameworks of higher dimensionality. The authors have also presented strong evidence for the important role played by H-bonds in the stabilization of open framework structures, which allow for the hierarchical assembly of homochiral porous solids.

Compounds **5**–**7** share the same feature in which the **L4** ligands bridge metal centers to form 1D zigzag or helical chains [12]. These 1D coordination chains are then further linked by interchain hydrogen bonding to form 2D or 3D networks. In compound **8**, the octahedral Cd atom is coordinated to four oxygen atoms of two chelating carboxylates of two different BDA ligands and two Cl atoms. The Cl ligands further bridge two Cd atoms giving Cd$_2(\mu\text{-Cl})_2$ units. The **L4** ligands play a bridging role between Cd$_2(\mu\text{-Cl})_2$ units to form 1D Cd$_4(\mu\text{-Cl})_4$(**L4**)$_2$. The OH groups of organic linkers are involved in H-bonding with oxygen atoms of the carboxylate groups linking 1D chains to four adjacent chains to give a 3D network. The network is highly porous with 59.1% of the crystal occupied by solvates and counterions. In compound **9**, the Cu$_2$(carboxylate)$_4$ units, described as paddle wheels, are bridged by binaphthyl backbones of each of the two **L4** groups to give 1D chains along the *b*-axis [13]. H-bonding between OH oxygen atoms and carboxylate O atoms of the 1D units links four neighboring chains to generate a 3D framework. The Cu$_4$(**L4**)$_4$ units are stacked on top of each other to create a porous network structure where MeOH and H$_2$O molecules reside.

A homochiral 1D Ni(II) phosphonate [Ni(**L5**-H$_2$)-(MeOH)$_4$], **10**, was obtained in 82.3% yield via a hydro(solvo)thermal reaction between 2NiCO$_3$·3Ni(OH)$_2$·

4H$_2$O and 2,2′-diethoxy-1,1′-binaphthylene-6,6′-bisphosphonic acid (**L5**-H$_4$) in methanol at 110 °C (Scheme 5) [14]. A single crystal X-ray diffraction study of (*R*)-**10** reveals the formation of a 1D zigzag coordination polymer consisting of 6-coordinate Ni center and bridging binaphthylbisphosphonate groups (Fig. 7). The Ni center adopts a slightly distorted octahedral geometry by coordinating to four methanol molecules and two oxygen atoms of two different binaphthylbisphosphonate ligands. The two phosphonate groups are monodeprotonated and coordinate to the Ni center in a *cis* geometry. The binaphthyl subunit has a dihedral angle of 115.49° and bridges adjacent Ni centers to form an infinite 1D zigzag chain running parallel to the *c*-axis. Adjacent chains of **10** pack in registry along the *a*-axis, however, 2$_1$ symmetry causes adjacent chains along the *b*-axis to adopt a staggered formation. The 1D structure of **10** is further stabilized by hydrogen bonding between phosphonic acid functionalities and coordinated methanol molecules to form a 3D H-bonded network.

Abruna and coworkers has designed an enantiomerically pure bridging ligand containing two 2,2′:6′,2″-terpyridine moieties (+ or −)-[ctpy-*x*-ctpy], **L6**, and synthesized redox-active homochiral 1D coordination polymers with both Ru^{2+} and Fe^{2+} metal connecting points (Scheme 6) [15,16]. When ligand (−)-[ctpy-*x*-ctpy] was treated with Fe(II) ion in EtOH and H$_2$O, a homochiral {(Fe((−)-[ctpy-*x*-ctpy])(PF$_6$)$_2$}$_n$ polymer was obtained. The Fe(II)/**L6** ratio of 1:1 was determined from UV-Vis spectrophotometric titration experiments. Both CD spectroscopic and scanning tunneling microscopic (STM) imaging studies support the formation of enantiopure structures (Fig. 8). A degree of polymerization of 60 was also estimated from the STM images on highly oriented pyrolytic graphite (HOPG). The two ctpy subunits in a single ligand cannot both coordinate to the same Fe(II) center in an octahedral fashion due to the steric constraints,
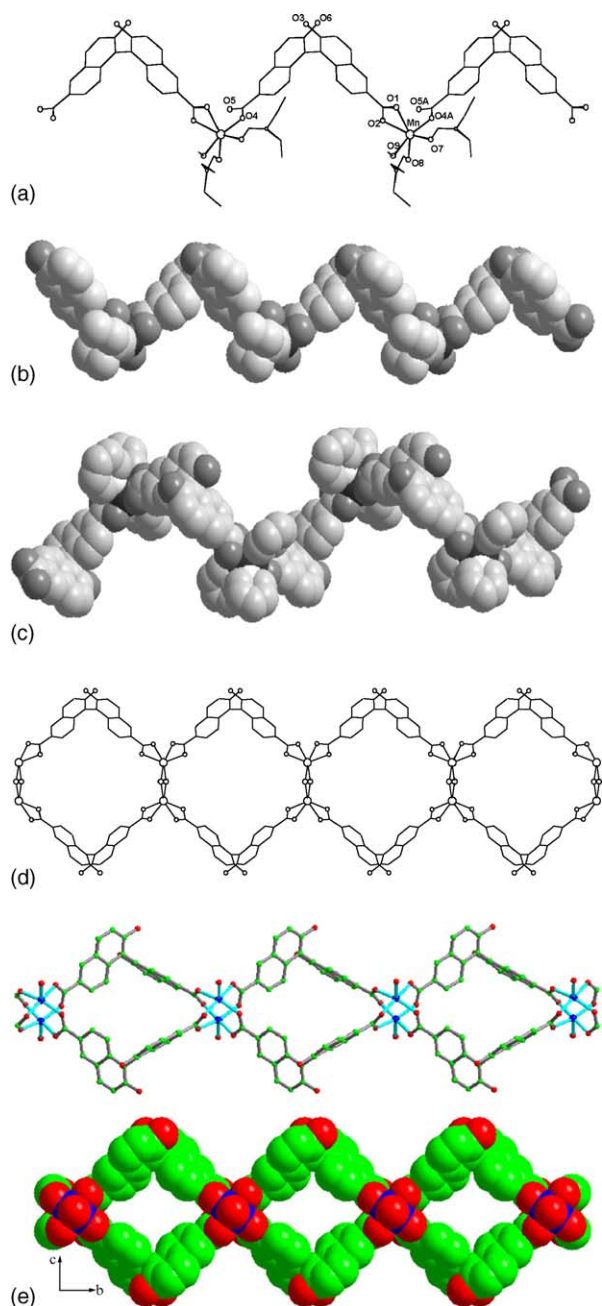
Fig. 6. (a) 1D zigzag chain of **5**; (b) space filling representations of 1D zigzag chain of **6**; (c) space filling representations of 1D helical chain of **7**; (d) 1D chains based on $Cd_4(\mu\text{-}Cl)_4(BDA)_2$ metallocycle in **8**; (e) ball and stick and space-filling model representations of 1D chains based on $Cu_2(carboxylate)_4$ in **9**.

and thus enforce the formation of homochiral 1D coordination polymer. Cyclic voltammetry and electrochemical quartz crystal microbalance (QCM) experiments on the polymers show reversible electrodeposition processes.

3.2. 2D homochiral MOCNs

The **L4** ligand with twisted dicarboxylate functionalities was also used to construct 2D homochiral MOCN [13].

$[HNMeEt_2]_2[Zn(\mathbf{L4})_2]\cdot 2MeOH\cdot 4H_2O$, **11**, was obtained in 36% yield by treating zinc nitrate and (*S*)-**L4**-H_2 in a mixture of *N,N'*-diethylformamide (DEF), MeOH and *N,N'*-dimethylaniline at 50 °C. The Zn center coordinates to four oxygen atoms of four monodentate carboxylate groups from four different **L4** ligands to adopt a distorted tetrahedral geometry. The **L4** ligands link adjacent Zn centers to form a corrugated 2D grid (Fig. 9). The 2D grids stack on top of each other in a staggered arrangement along the *c*-axis with a layer-to-layer separation of 7.17 Å. Such a staggered arrangement allows the OH groups and uncoordinated carboxylate oxygen atoms from adjacent layers to form strong interlayer H-bonds. Compound **11** thus adopts an interesting homochiral porous network structure with open channels running along both *a*- and *b*-axes. These open channels are occupied by two $[HMeNEt_2]^+$ counter ions and four water and two methanol guest molecules per formula unit.

Lin and coworkers has recently used a BINOL-derived dicarboxylate ligand of a different configuration to construct 2D chiral MOCNs [17]. Reactions of enantiopure 6,6'-dichloro- 2,2'-diethoxy-1,1'-binaphthylene-4,4'-dicarboxylic acid (**L7**-H_2) with appropriate metal salts in DMF, MeOH and pyridine at 60 °C afforded a series of isostructural homochiral porous 2D metal carboxylates of the general formula $[M_2(\mu\text{-}H_2O)(\mathbf{L7})_2(py)_3(DMF)]\cdot(DMF)\cdot(H_2O)_x$ (M: Mn, *x* = 2; Co, *x* = 3; Ni, *x* = 3), **12a–c** (Scheme 7). Single crystal X-ray structural studies on **12a** reveal a 2D network that crystallizes in the chiral space group $P2_12_12_1$.

The basic building unit for **12a–c** can be viewed as two metal centers bridged by one H_2O molecule and two carboxylate groups of two different **L7** ligands. One DMF and three pyridine molecules complete the coordination geometry around the metal centers. This dimetal carboxylate unit is further linked to four neighboring dimetal cores through the carboxylate groups on the 4,4' positions of four different **L7** ligands. As a result, a 2D neutral rhombohedral grid is constructed that have chiral cavities (Fig. 10). The ethoxy protected BINOL functionality in the network structure is oriented toward the chiral pores. However, the void space in **12a–c** is minimal as the 2D grids have a staggered arrangement with a 7.45 Å layer to layer separation and is occupied by one DMF and two water molecules.

In a separate work, Lin and coworkers prepared a homochiral 2D Zn(II) phosphonate $[Zn_3(\mathbf{L5}\text{-}H)_2(C_6H_5N)_2]$, **13**, via a hydro(solvo)thermal reaction of enantiopure **L5**-H_4 and $Zn(ClO_4)_2\cdot 6H_2O$ in MeOH, H_2O, and pyridine at 110 °C [14]. Single crystal X-ray diffraction studies revealed a 2D network with two distinct tetrahedral Zn^{2+} centers in **13**. Zn(1) is coordinated to a pyridine molecule and three oxygen atoms of three different **L5**-H ligands, while Zn(2) is coordinated to four oxygen atoms of four different bisphosphonate ligand. The Zn centers are bridged in a μ_2,η^2 fashion by monodeprotonated phosphonate group and μ_3,η^3 fashion by doubly deprotonated phosphonate group to form infinite chains of $[Zn(\mu_2,\eta^2\text{-}PO_3H)_2\cdot Zn_2(\mu_3,\eta^3\text{-}PO_3)_2(py)_2]_\infty$ along *b*-axis
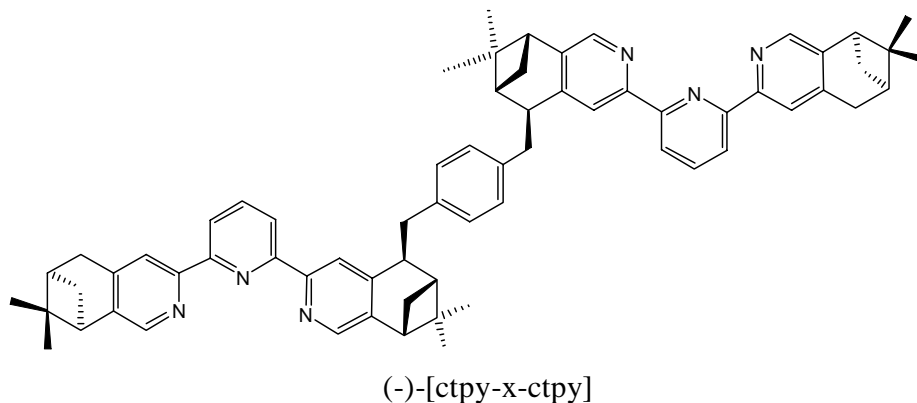
Scheme 5.

(a)

(b)
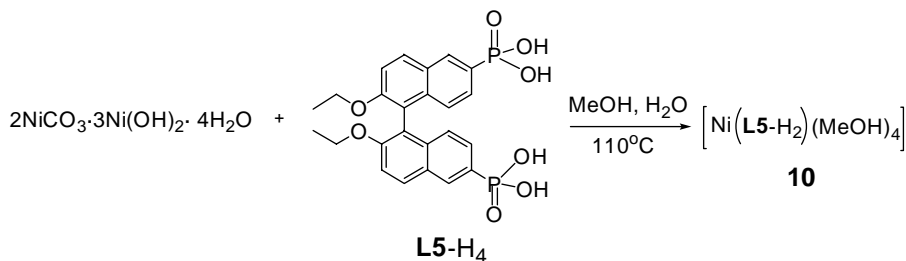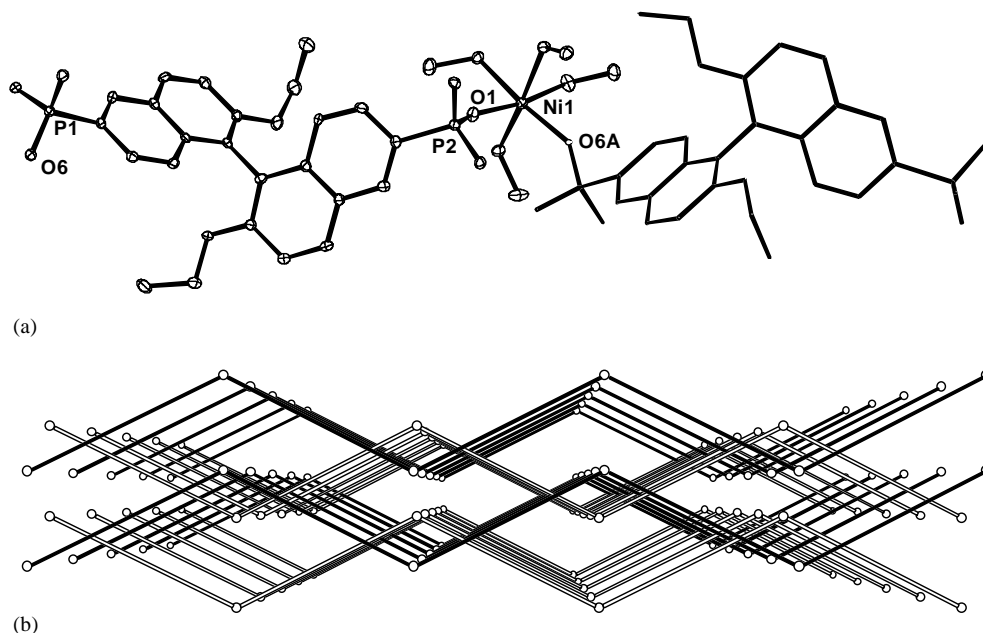
Fig. 7. (a) Coordination environment of **10** and (b) view of the zigzag framework along *b*-axis.

which are further bridged by **L5**-H ligands to lead to an infinite 2D grid in the *ab* plane (Fig. 11). The coordinated pyridines interdigitate via π–π stacking to give a nonporous solid.

Based on earlier findings that combination of Ag(I) ions and C$_3$ symmetric 1,3,5-tris(4-ethynylbenzonitrile)benzene lead to AlB$_2$ type honeycomb 2D networks, Lee and coworkers systematically varied the pendant group of this tris(nitrile)benzene ligand [18]. A combination of single crystal and powder X-ray diffraction studies clearly established that all the solids with varying pendant groups adopt the same network structure. These modifications resulted

(-)-[ctpy-x-ctpy]

Scheme 6.
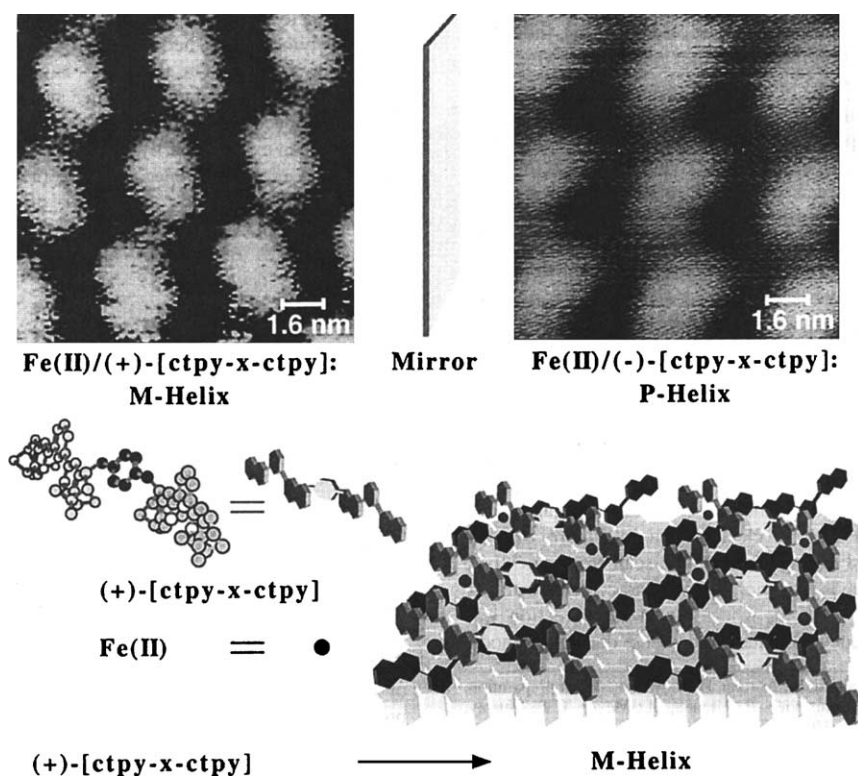
Fig. 8. High resolution STM image of highly ordered arrays of (±)**L6** and Fe(II). Energy optimized structure of (+)-[ctpy-*x*-ctpy] and a rendition of the helical structure formed from **L6** and Fe(II).

in porous silver coordination networks with channel sizes varying from 15 to 25 Å in diameter. More importantly, 1,3,5-tris(4-ethynylbenzonitrile)benzene with chiral (1*S*, 2*S*, 5*S*)-Myrtanoxy pendant was also prepared (Scheme 8) and used to construct a homochiral 2D Ag coordination network of the AlB_2 structure type which has eclipsed planar honeycomb sheets (Fig. 12).

Bodwin and Pecoraro have designed and synthesized many chiral metallacrowns that could be used as a building block for the construction of homochiral MOCNs [19]. 2D chiral $\{Cu^{II}(NO_3)_2[12MC_{Cu^{II}N(S-\beta-pheHA)}-4]:Cu_2(benzoate)_4\}$, **14**, was prepared from a MeOH solution of phenylalaninehydroxamic acid, sodium benzoate and $Cu(NO_3)_2$. It is evident from single crystal X-ray diffraction studies that the metallacrowns are linked by $Cu_2(benzoate)_4$ dimers to each other via the carbonyl oxygen of the hydroximate moiety to yield a linear chain of [MC-Cu$_{dimer}$]$_n$ units. The 2D structure arises from further linking of these linear chains by bridging nitrate ligands (Fig. 13). The 2D framework contains channels with dimensions of ∼8 Å × 9 Å. A closer examination of the structure indicates that the sides of the channels are generated from overlap of aromatic rings whereas the metallacrown units make up the top and bottom layers. The benzoic acid guest molecule resides in the cavities and H-bonds to the framework. A similar structure was obtained when the synthesis was carried out in the absence of nitrate ions. The lack of nitrate bridges mainly enables closer packing of the [MC-Cu$_{dimer}$]$_n$ linear chains.

The arrangement of the phenyl groups in the [MC-Cu$_{dimer}$]$_n$ units was proposed to be the reason for the presence of channels, as the nitrate-free structure has the same channel size and orientation.

To synthesize chiral porous square grid coordination polymers, Bunz and zur Loye developed a bipyridine-type ligand with chiral functionality and a long side chain to avoid interpenetration [20]. Reaction of the chiral 9,9-bis[(*S*)-2-methyl-butyl]-2,7-bis(4-pyridylethynyl)fluorene ligand, **L8**, with $Cu(NO_3)_2$ in EtOH/CH_2Cl_2 solvent mixture yielded [Cu(**L8**)$_2$(NO$_3$)$_2$], **15** (Scheme 9). A single crystal X-ray diffraction study shows that **15** crystallizes in the chiral space group $P2_1$ with an ABCABC layer arrangement of noninterpenetrating square grids. The square grids in this coordination polymer are undulating and nonplanar. The fluorene side chains of the ligands have identical arrangement on all the grid sides and point inside the channels to reduce the void space (Fig. 14). The open channel size is thus only ∼8 Å × 8 Å, even though the grid dimensions are ∼25 Å × 25 Å^2. Calculations with PLATON gave 11.8% free volume that is filled with solvent molecules [21].

Ngo and Lin also incorporated a chiral crown ether moiety into the bridging bisphosphonate ligand to form homochiral porous lamellar lanthanide bisphosphonates [22]. Enantiopure 2,2′-pentaethyleneglycol-1,1′-binaphthyl-6,6′-bisphosphonic acid (**L9**-H$_4$) was treated with lanthanide salts in acidified MeOH solution at room temperature to give
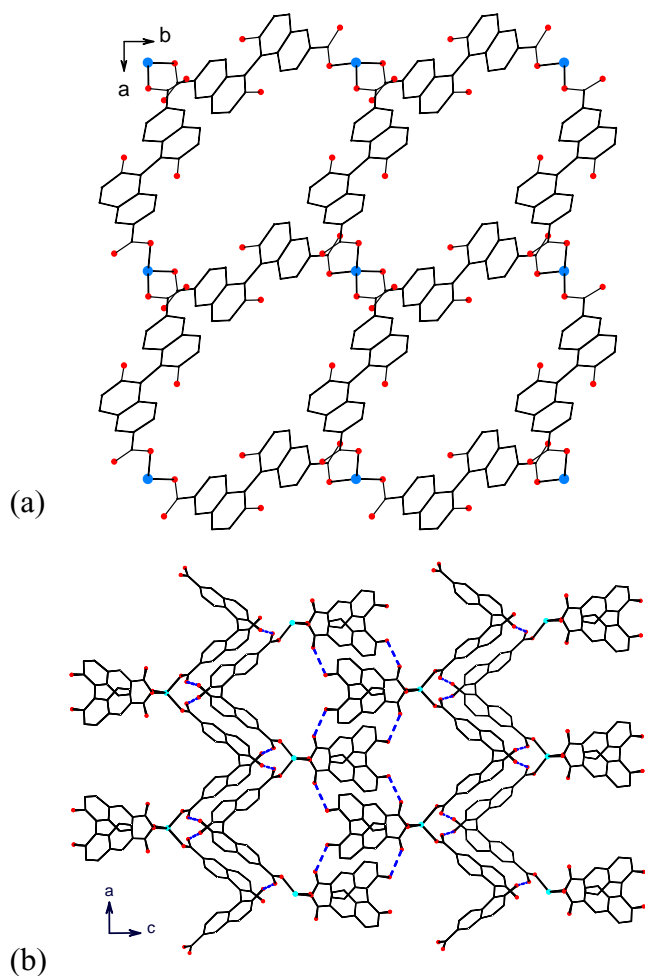
Fig. 9. (a) A view of 2D rhombohedral grid of **11** down the *c*-axis. (b) 3D H-bonded open framework of **11** down the *b*-axis.
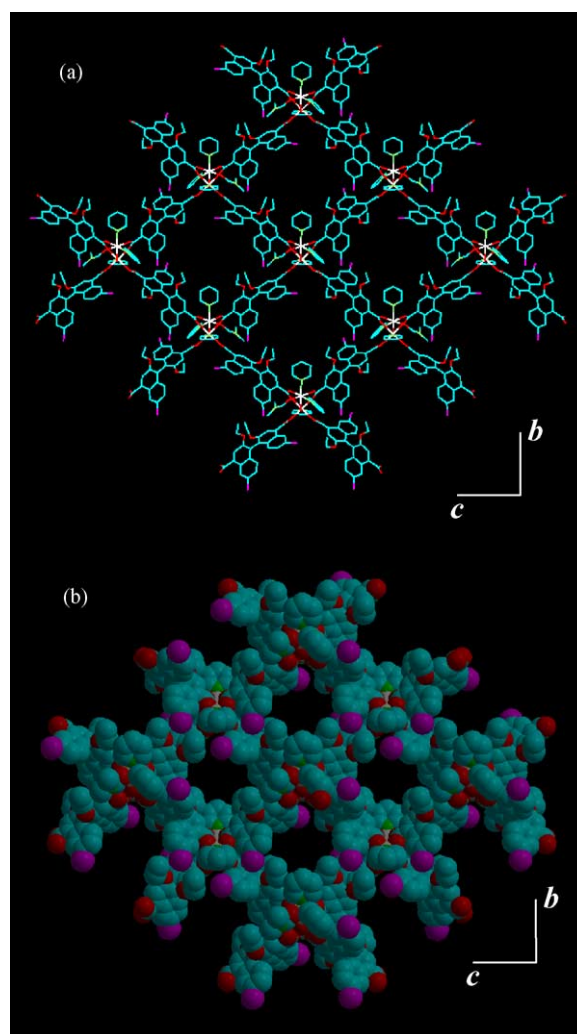

Fig. 10. (a) Crystal structure of **12a**, showing the 2D rhombohedral grid and (b) space filling model down the *a*-axis.

lamellar solids with the general formula $[Ln_2(\mathbf{L9}\text{-}H)_2$ $(MeOH)_8]\cdot(\mathbf{L9}\text{-}H_4)\cdot(HCl)_3\cdot(H_2O)_6$, **16** (Scheme 10).

Single crystal X-ray diffraction studies of the Nd compound show a 2D lamellar structure where the chiral crown ether groups are present between the phosphonate layers. The Nd centers in **16** adopt a square anti-prismatic geometry by coordinating to four methanol molecules and four phosphonate oxygen atoms of four different **L9**-H ligands. Both phosphonate groups of the **L9**-H ligand adopt a κ_2,μ_2 binding mode, and link adjacent Nd centers to form doubly

bridged 1D lanthanide phosphonate chains along the *b*-axis. The binaphthyl backbones of the **L9**-H ligands link adjacent 1D lanthanide phosphonate chains to form a 2D coordination network lying in the *ab* plane (Fig. 15). The lamellae of **16** are however intercalated with free **L9**-H$_4$ molecules, and as a result, there is only enough void space in **16** to accommodate three hydrogen chloride and six water molecules per formula unit. The limited porosity of **16** has thus precluded its application in bulk chiral separations. Nonetheless, **16**
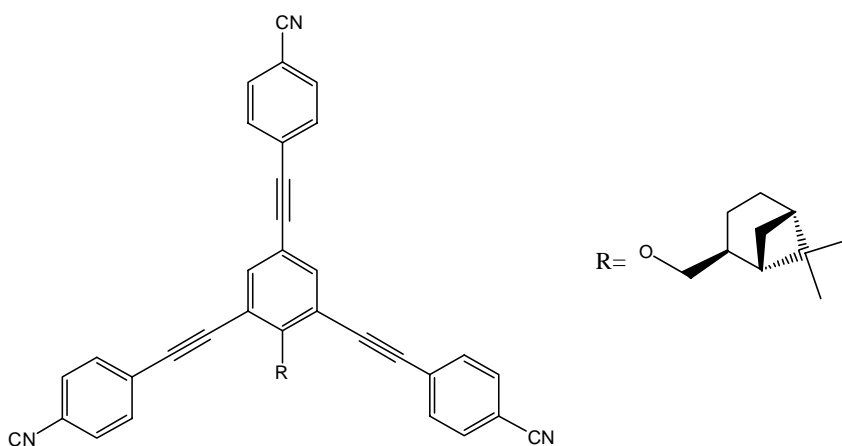

Scheme 7.

(a)

(b)
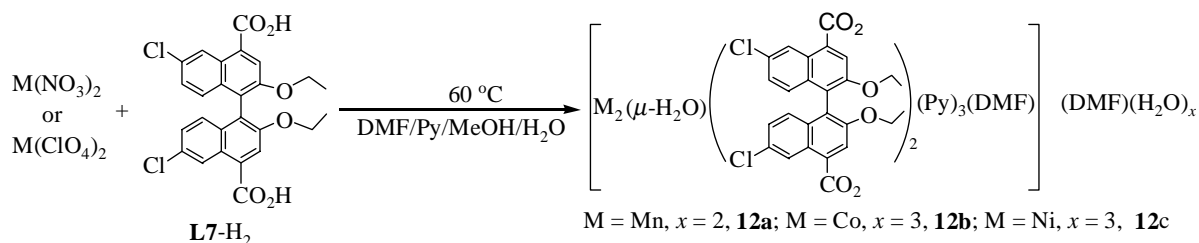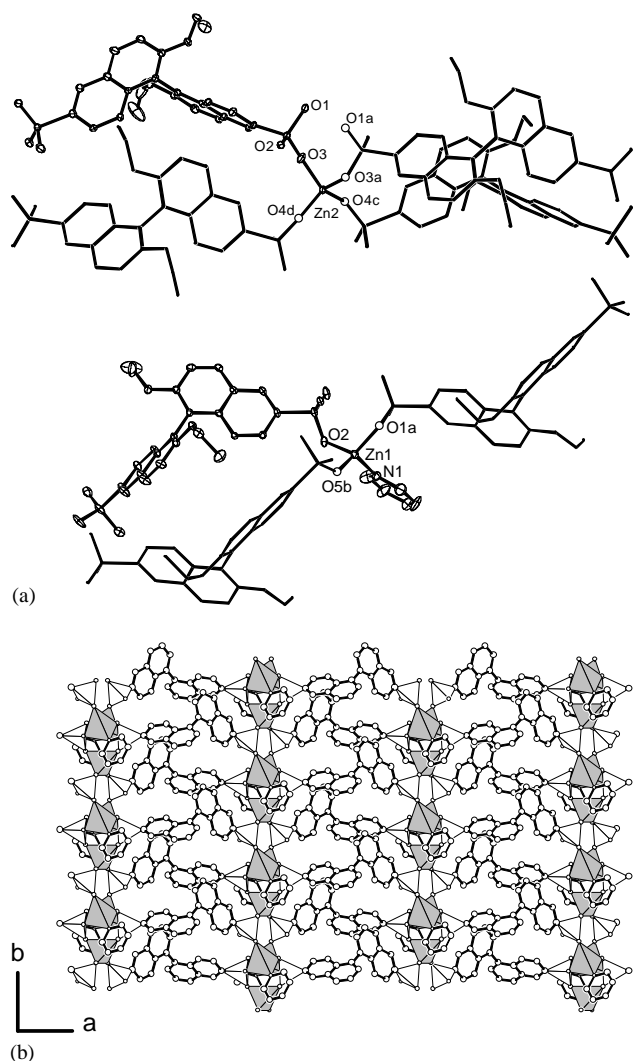
Fig. 11. (a) Coordination environments of Zn and (b) 2D network along *c*-axis of [Zn$_3$(**L5**-H)$_2$(C$_6$H$_5$N)$_2$].

represents an interesting structural model for chiral porous materials that can be used for bulk chiral separations.

3.3. 3D homochiral MOCNs

Ranford et al. reported an interesting route to homochiral 3D MOCNs via topochemical conversion of H-bonded networks [23,24]. By employing chiral amino acid-derived bridging ligand *N*-(2-hydroxybenzyl)-L-alanine (H$_2$sala), H-bonded network [{Zn(sala)(H$_2$O)}$_2$]·2H$_2$O, **17**, was obtained [23]. The Zn centers have square pyramidal geometry where sala ligand coordinates to the metal centers via N atom of the amine moiety, O atoms of the carboxylate group, and the bridging phenolato group (Fig. 16). Compound **17** adopts a 3D H-bonded structure with chiral channels that are occupied by water molecules. Interestingly, upon heating, **17** dehydrated and underwent topochemical conversion to give a homochiral 3D MOCN [{Zn(sala)}$_n$], **18**. With the exception of the extrusion of both coordinated and solvating water molecules, **18** retained the network structure of **17** with Zn-carboxylate bonds in **18** replacing hydrogen bonds in **17** (Scheme 11). A homochiral 3D Cu(II) MOCN that is isostructural to **18** was also obtained in a similar topochemical conversion [24]. This work represents a rare example of "solid-state supramolecular synthesis" of a MOCN.

Lin and coworkers demonstrated the increase of dimensionality of a homochiral MOCN by using lanthanide metals that have higher coordination numbers than first-row transition metals [25]. Homochiral lanthanide carboxylates with the general formula of [Ln$_2$(**L7**)$_3$(DEF)$_2$(py)$_2$]·2DEF·5H$_2$O (Ln: Gd, Er, Sm, **19a–c**; DEF: *N,N′*-diethylformamide; py: pyridine) were prepared in 30–45% yields by treating hydrated lanthanide salts and **L7**-H$_2$ in a mixture of DEF, MeOH and Py at 50 °C. The basic building unit for **19a** contains two crystallographically equivalent Gd centers that are quadruply bridged by four carboxylate groups of four **L7** ligands (Fig. 17). Each Gd center also coordinates to a chelating carboxylate group of a **L7** anion, a DEF molecule, and
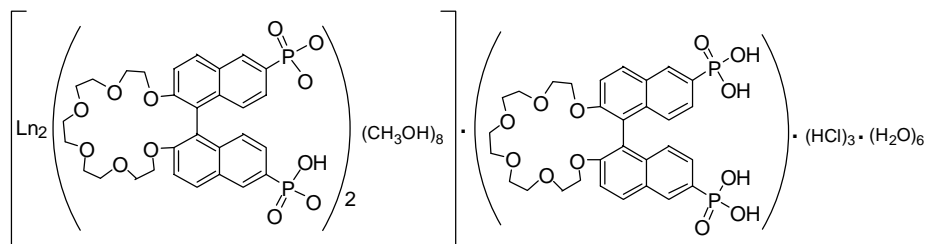

Scheme 8.
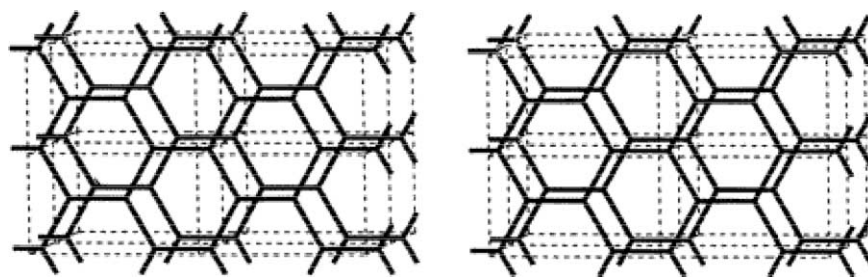
Fig. 12. 2D boron net in AlB$_2$.
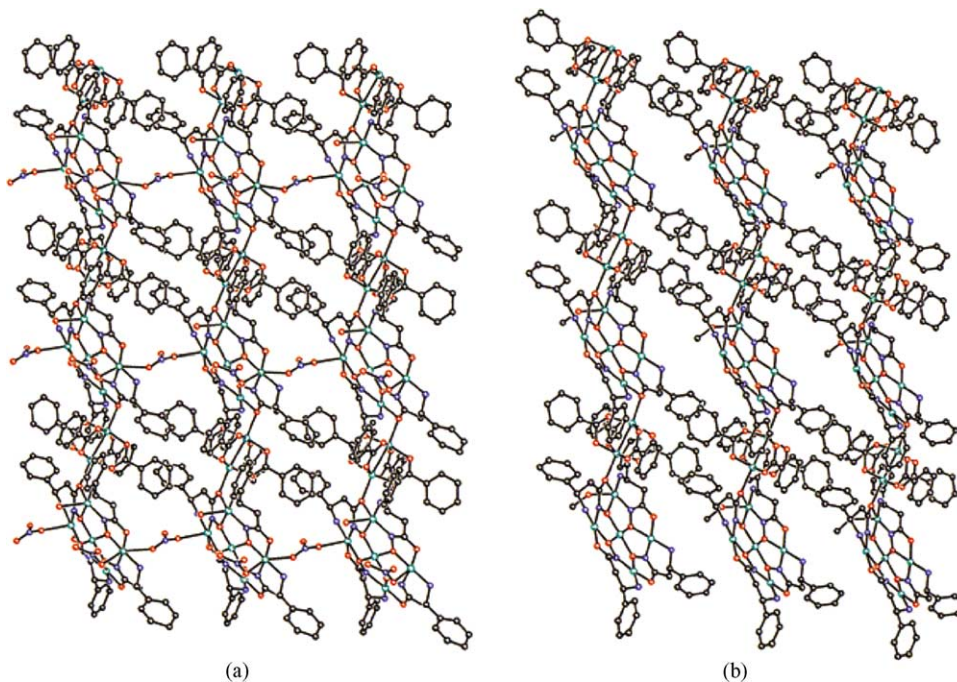
Fig. 13. 2D network of **14** (a) with nitrate bridges and (b) nitrate-free structure.

L8
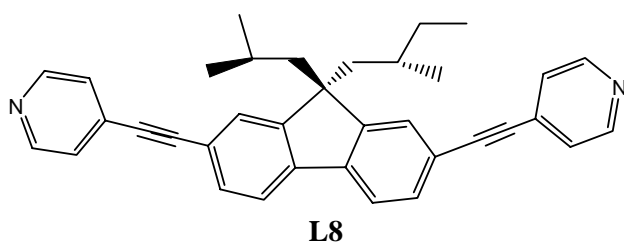
Scheme 9.

a pyridine molecule to afford a distorted square antiprism geometry.

Each digadolinum core in **19a** is linked by six **L7** ligands to six adjacent digadolinum cores to form two independent hexagonal 6^3 grids in the *ab* and *ac* planes, respectively, and result in a unique 3D neutral framework with a 1D channel running parallel to the *a*-axis, as shown in Fig. 17. The structure can be classified as a 4^{9}6^6 topological type

Ln = Nd, **16a**, or Sm, **16b**

Scheme 10.
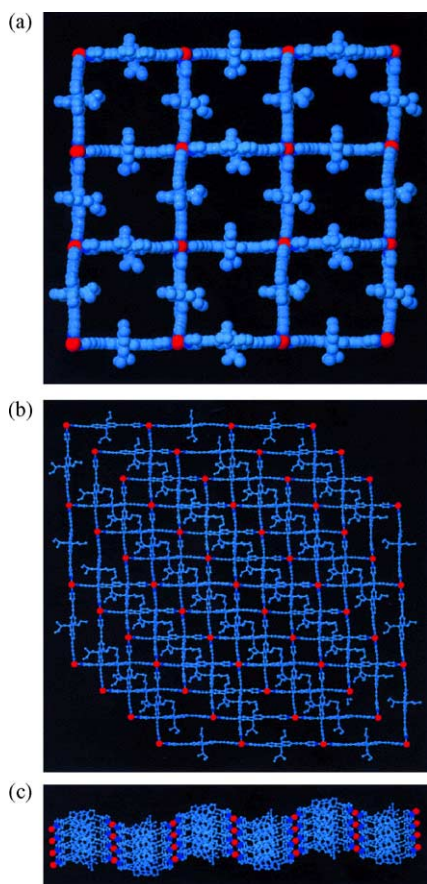
Fig. 14. (a) Single square grid of **15**; (b) stack of four square-grid layers showing 8 Å × 8 Å channels; (c) undulating orientation of four adjacent stacked grids.

built upon six-connected nodes as defined by Wells. Both the ethoxy-protected BINOL functionalities and the chlorine atoms are pointing towards the channel, leading to an asymmetric 1D channel with a cross-section of ∼3.1 × 6.2 Å that is occupied by two DEF and five water guest molecules.

Lin and coworkers recently reported interesting 3D homochiral MOCNs built from axially chiral bipyridines [26]. When C_2 symmetric 1,1′-binaphthyl-6,6′-bipyridine ligands **L10** or **L11** was reacted with Ni(acac)$_2$ in
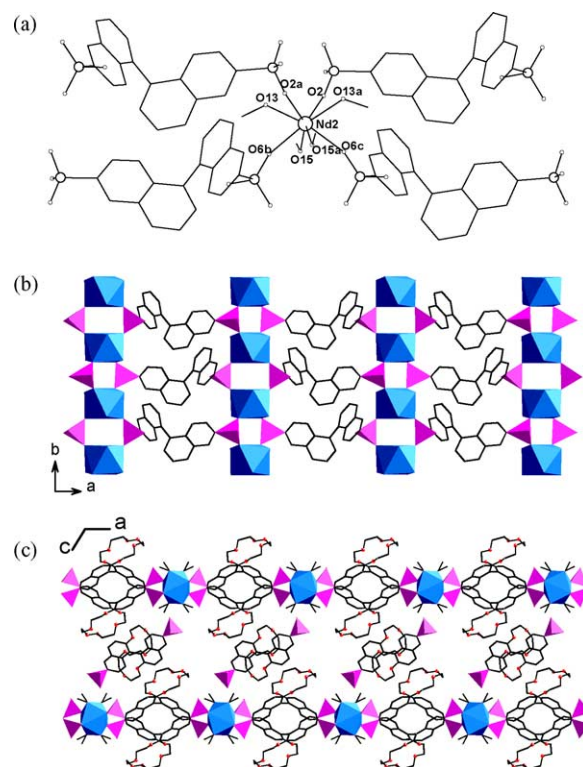
Fig. 15. Crystal structure of [Nd$_2$(**L9**-H)$_2$(MeOH)$_8$]·(**L9**-H$_4$)·(HCl)$_3$· (H$_2$O)$_6$. (a) Coordination environment at Nd center; (b) view of the lamellar structure; (c) another view of the lamellar structure showing the pendant crown ethers and free **L9**-H$_4$ molecules.

CH$_2$Cl$_2$/CH$_3$CN solvent mixtures at 70 °C for 2 days, periodically ordered homochiral interlocked nanotubes [Ni(acac)$_2$(**L10**)]·3CH$_3$CN·6H$_2$O, **20** and [Ni(acac)$_2$(**L11**)]· 2CH$_3$CN·5H$_2$O, **21**, were obtained (Scheme 12). The chiral framework results from the assembly of interlocking quintuple helices. The **L10** ligand bridge the Ni(acac)$_2$ units to result in an infinite helical chain along the c-axis where a tetragonal nanotube is formed due to parallel alignment of five infinite helical chains (Fig. 18). 3D chiral framework is a result of the interlocking of these nanotubes where the corners of the nanotubes are partially eclipsed to give chiral pores with 1.7 nm × 1.7 nm dimensions. Smaller channels
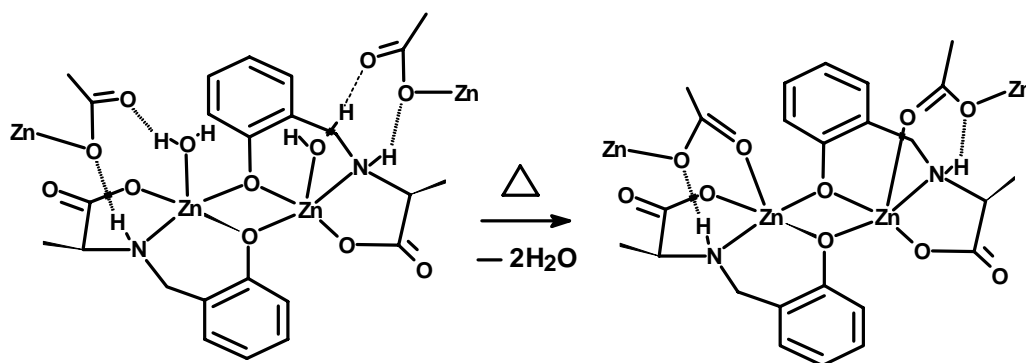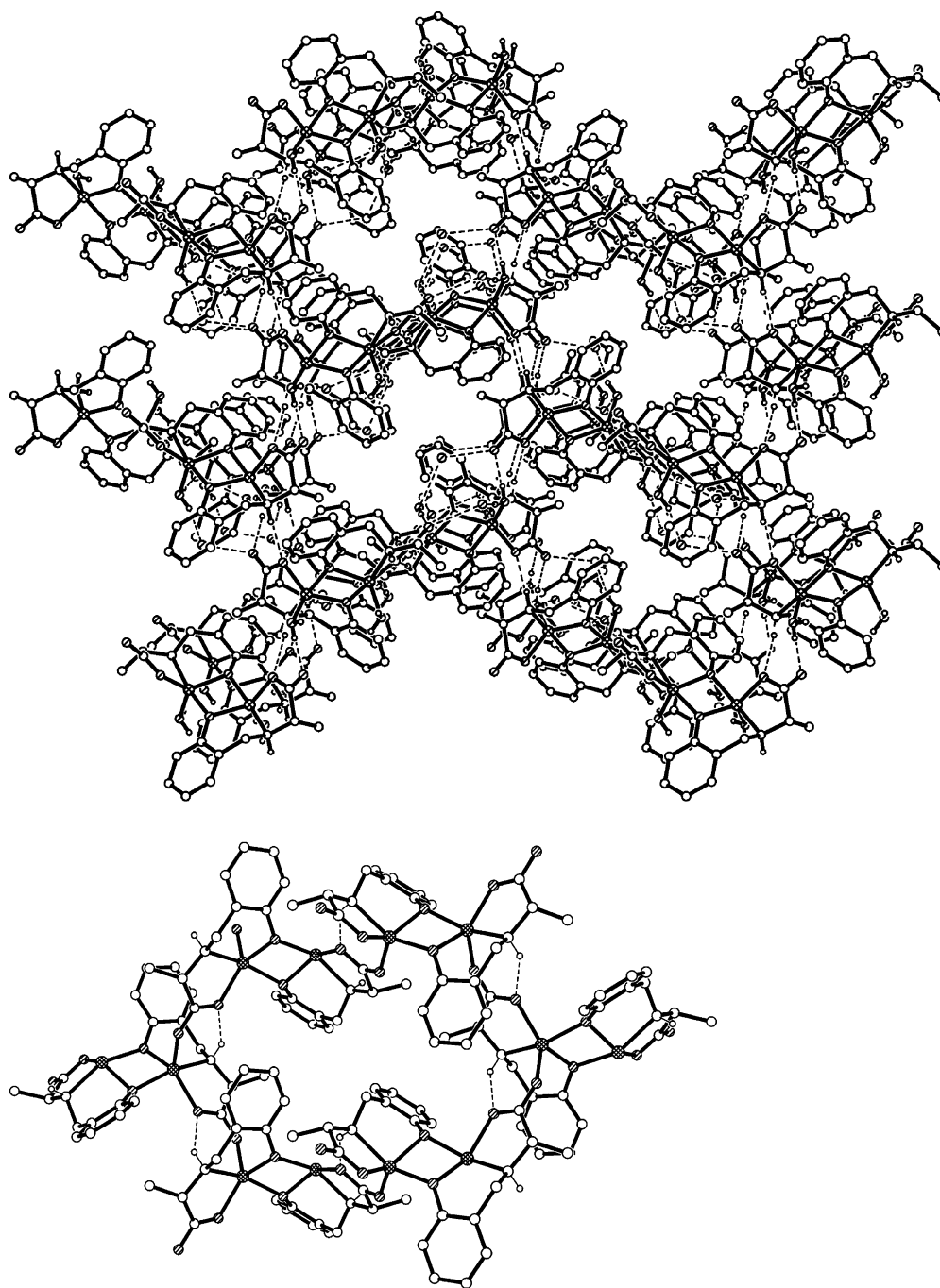

Scheme 11.

Fig. 16. 3D structure of (top) [{Zn(sala)(H$_2$O)}$_2$]·2H$_2$O, **17** and (bottom) [Zn$_2$(sala)$_2$], **18**.

of the size 7 Å × 11 Å exist in the structure, all containing H$_2$O and CH$_3$CN solvate molecules. The inclusion volume is 45.4% of the total volume as determined from PLATON calculations on the solvent-free structure [21].

The chiral crown ether functional groups on **L11** were successfully introduced into the nanotubes in [Ni(acac)$_2$(**L11**)]·2CH$_3$CN·5H$_2$O. The chiral crown ether groups are at the sides of the channels and are oriented into the neighboring tubes in the 3D framework. H$_2$O and CH$_3$CN occupy the channels that make up ∼40% of the

crystal volume. The presence of chiral crown ethers at the sides of the channels could be explored for chiral separations. Both **20** and **21** show framework stability toward the removal of solvent molecules.

Lin and coworkers also constructed homochiral 3D MOCNs using chiral bisphosphonic acid [14]. Hydro(solvo)thermal reactions of **L5**-H$_4$ with MnCO$_3$ and CoCO$_3$ in H$_2$O and MeOH solvent mixtures at 110 °C yielded homochiral [Mn(**L5**-H$_2$)](MeOH)]·MeOH, **22**, and [Co$_2$(**L5**-H$_2$)$_2$(H$_2$O)$_3$]·(H$_2$O)$_4$, **23**, respectively. Both **22**
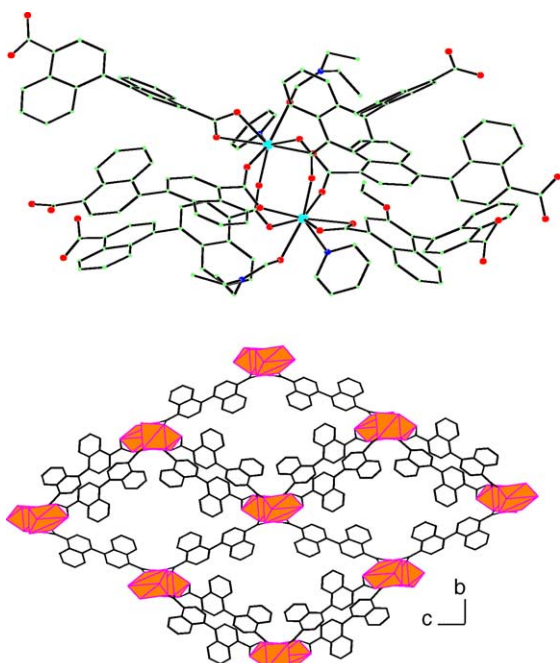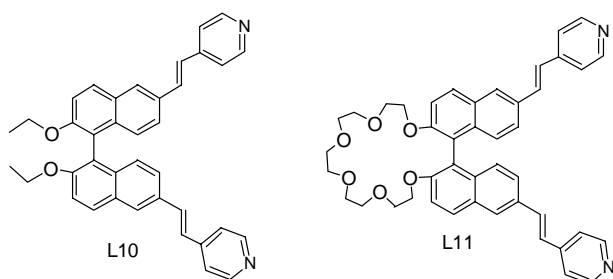
Fig. 17. (Top) Digadolinium building unit of **19a** and (bottom) polyhedral presentation of the 3D network of **19a** along the *a*-axis.
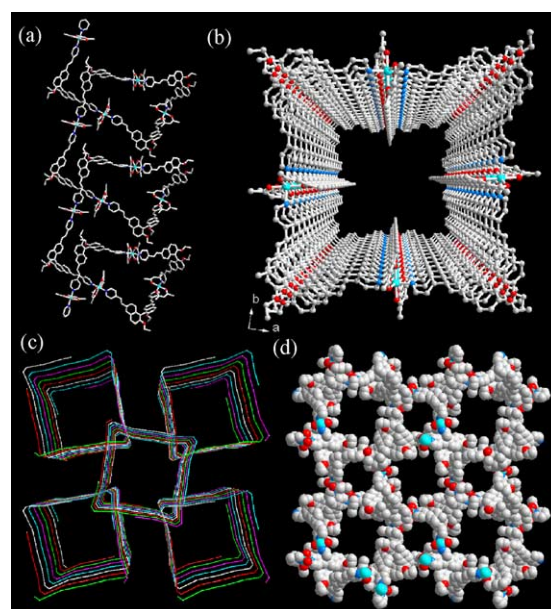

Fig. 18. Views of (a) the helical chain; (b) the nanotube made of five parallel helices; (c) interlocking adjacent helices; (d) space filling model showing the open channels in 3D network of [Ni(acac)$_2$(**L10**)].

and **23** exhibit 3D network structures, and contain chiral cavities.

The Mn atom in **22** is five coordinate with one MeOH and four oxygen atoms of four different **L5**-H$_2$ ligand. The phosphonate groups of **L5** link adjacent Mn atoms to form [Mn(PO$_3$H)$_2$]$_\infty$ chains along the *a*-axis (Fig. 19). These [Mn(PO$_3$H)$_2$]$_\infty$ chains are further linked by bridging **L5**-H$_2$ groups to form a homochiral 3D network. The 3D framework contains rhombohedral channels with approximate dimensions of 5.3 Å × 2.7 Å, filled with MeOH guest molecules.

There are two distinct Co atoms in **23** with different co-ordination geometries. The Co1 center has a distorted oc-tahedral geometry, by coordinating to three oxygen atoms of three **L5**-H$_2$ in a *fac* configuration and to three H$_2$O molecules. The Co2 center has a tetrahedral geometry by coordinating to four oxygen atoms of four different **L5**-H$_2$ groups (Fig. 20). Two of three phosphonate bridge the same two Co atoms to give dimetal units which are further con-nected to each other by the third phosphonate bridging group

to form infinite [Co(H$_2$O)$_3$(PO$_3$H)$_2$·Co(PO$_3$H)$_2$]$_\infty$ helical chains along the *b*-axis. These helical chains are then linked by binaphthyl backbones to lead to a homochiral 3D net-work. The resulting 3D framework is porous with rhombo-hedral pores of 3.4 Å × 4 Å that are filled with four H$_2$O molecules.

A nonporous 3D network of the formula [Cu(**L5**-Et)$_2$], **24**, was also prepared hydrothermally from CuO and **L5**-H$_4$ bridging ligand in ethanol. Interestingly, the PO$_3$Et species has formed under these conditions, apparently a result of in situ esterification of **L5**-H$_4$ to give **L5**-Et$_2$. Four different **L5**-Et$_2$ ligands are coordinated to Cu center giving rise to a distorted square planar geometry. [Cu(PO$_3$Et)$_2$]$_\infty$ infinite chains are generated along the *a*-axis by bridging adjacent Cu centers with phosphonate groups (Fig. 21). Similar con-nectivity of infinite chains as observed in the Mn structure affords a homochiral 3D MOCN with rhombohedral chan-nels which are completely occupied by the ethoxy groups.

4. Homochiral MOCNs for enantioselective processes

Although Fujita et al. [27] and Aoyama and coworkers [28] used coordination networks as Lewis acids for het-erogeneous catalysis, Kimoon and coworkers reported the first example of asymmetric catalysis using a homochi-ral MOCN [29]. Enantiopure bridging ligand **L12** with both carboxylic and pyridyl functional groups was derived from readily available D-tartaric acid, and treated with Zn(NO$_3$)$_2$ in a H$_2$O/MeOH solvent mixture to give porous and chiral [Zn$_3$(μ$_3$-O)(**L12**-H)$_6$]·2H$_3$O·12H$_2$O (D-POST-1)

Scheme 12.
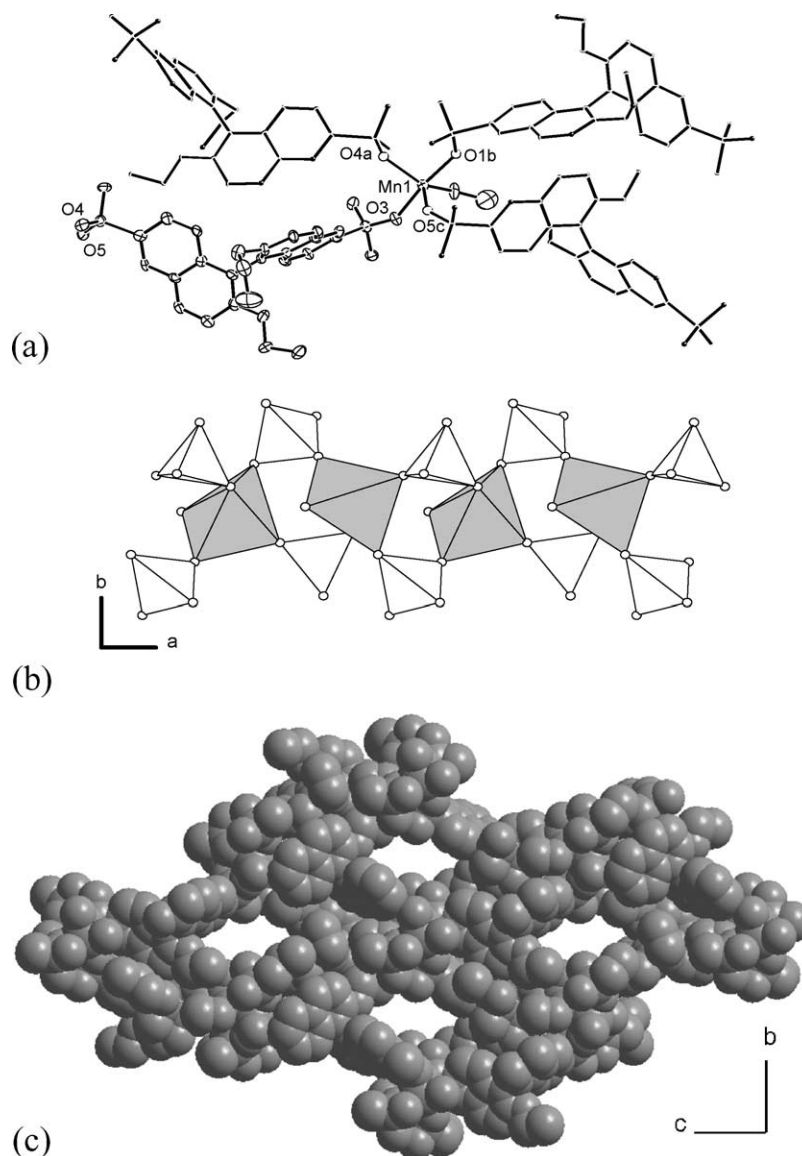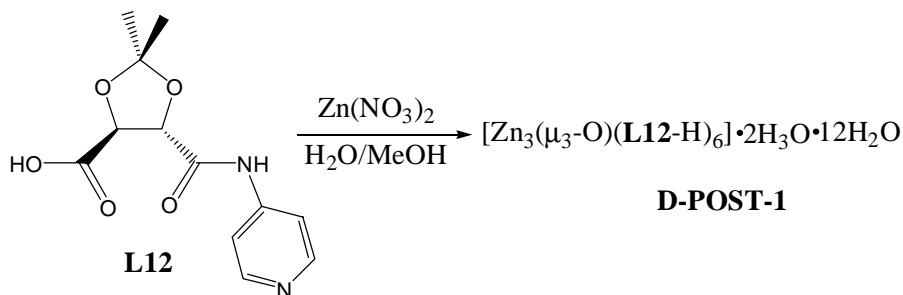
Fig. 19. (a) Coordination environment of **22**; (b) view of the infinite [Mn(PO$_3$H)] chains along *a*-axis; (c) space filling model of **22**.

(Scheme 13) [29]. In D-**POST**-1, three zinc ions are held together with six carboxylate groups of the deprotonated chiral ligands **L12** and a bridging oxo oxygen, to form a trinuclear unit, in which a three-fold axis parallel to the *c*-axis passes through the center of the trinuclear unit (Fig. 22). The trinuclear units in **POST**-1 are interconnected through three pyridyl groups of **L12** to generate 2D infinite layers consisting of large edge-sharing chair-shaped hexagons
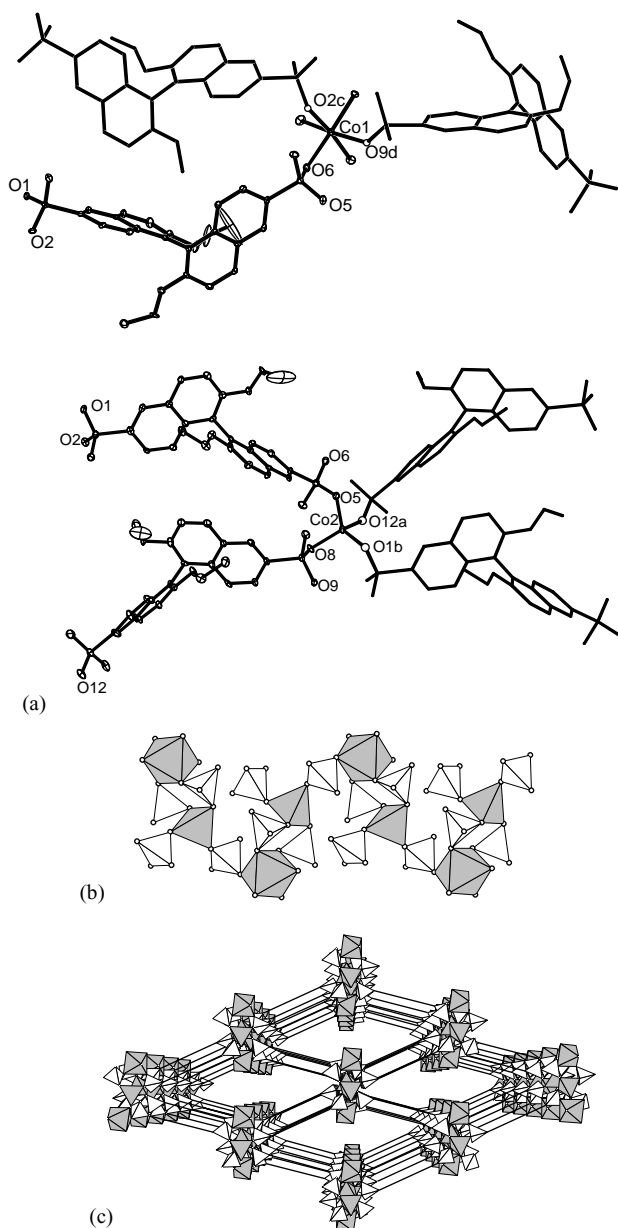

Scheme 13.

Fig. 20. (a) Coordination environment of **23**; (b) view of the infinite $[Co(H_2O)_3(PO_3H)_2 \cdot Co(PO_3H)_2]$ chain in **23** along the c-axis; (c) view of the 3D framework of **23** along the b-axis.

with a trinuclear unit at each corner (Fig. 23). The 2D layers stack along the c-axis with an interlayer spacing of 15.47 Å. Interestingly, large chiral 1D channels exist along the c-axis, which can be best described as an equilateral triangle with a side length of ~13.4 Å. The void volume of the channels of **POST**-**1** is estimated to be ~47% of the total volume and is filled with 47 water molecules per unit cell. **POST**-**1** loses crystallinity upon removal of the solvate molecules by evacuation, but the X-ray powder diffraction pattern of **POST**-**1** can be regenerated upon exposing the evacuated sample to ethanol or water vapor.

Three of six pyridyl groups in each trinuclear unit $([Zn_3(\mu_3\text{-}O)(\textbf{L12}\text{-}H)_6]^{2-})$ are coordinated to the zinc ions

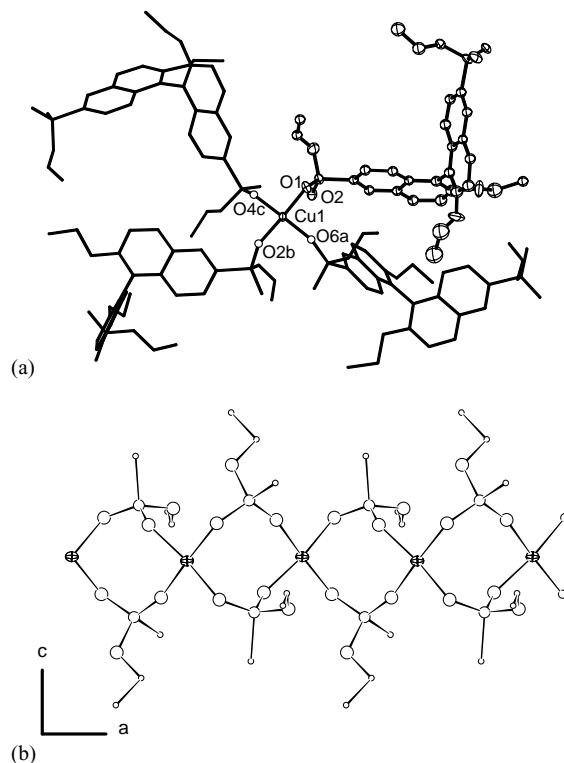
Fig. 21. (a) Coordination environment of **24** and (b) view of the infinite $[Cu(PO_3Et)_2]$ chains along the c-axis.

of three neighboring trinuclear units. The other three extrude into the channel without any interactions with the framework. Charge neutrality argument would suggest that two of the three dangling pyridyl groups have been protonated, which has been supported by elemental analysis. The protons bound to the pyridyl groups can be exchanged with alkali metal ions, which is consistent with the protonated nature of the two pyridyl groups. Interestingly, the pore size of **POST**-**1** can be varied by N-alkylation of the pyridyl groups. TGA results suggest that the pore volume of **POST**-**1** shrinks by 14 and 60% upon N-alkylation with iodomethane and 1-iodohexane, respectively.

The presence of accessible chiral pores in D-**POST**-**1** allows enantioselective inclusion studies. Enantioselective inclusion of chiral metal complexes was studied by using racemic $[Ru(2,2'\text{-bipy})_3]Cl_2$ and EtOH suspension
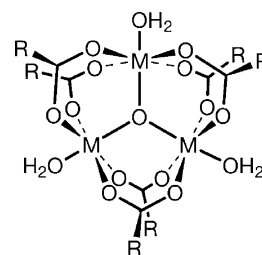
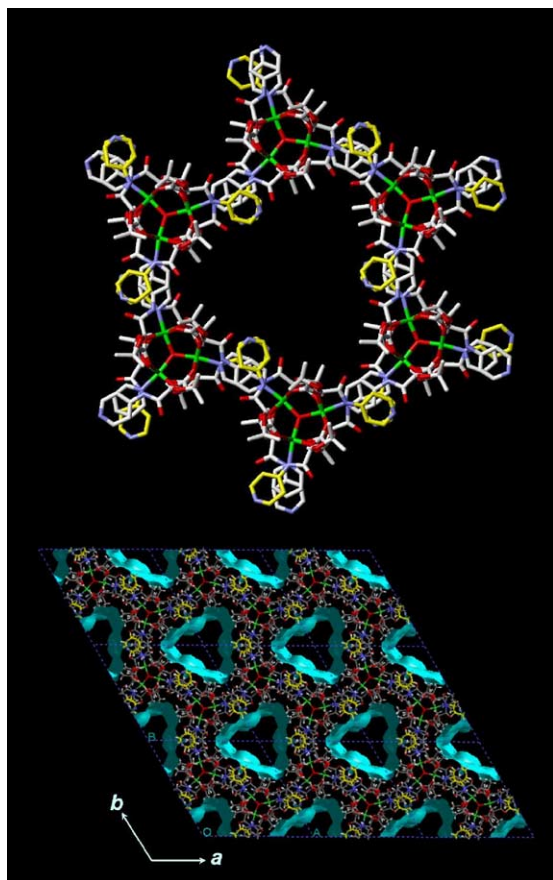

Fig. 22. Trinuclear building unit in **POST**-**1**.

Fig. 23. (Top) The hexagonal framework of **POST**-1 that is formed with the trinuclear SBU and (bottom) the chiral trigonal channels of **POST**-1 as viewed down the *c*-axis.

of L-**POST**-1. [Ru(2,2′-bipy)₃]Cl₂ was exchanged with the 80% of the protons on the pyridyl groups enantios-electively, with an enantio excess of 66% in favor of Δ isomer.

The dangling pyridyl groups in **POST**-1 were used to catalyze transesterification reactions. While the reaction of **25** and ethanol in the presence of **POST**-1 in carbon tetra-chloride for 55 h at 27 °C produced ethyl acetate in 77% yield, no or little transesterification occurs without **POST**-1 or with the *N*-methylated **POST**-1, respectively. Transes-terification of **25** with bulkier alcohols such as isobutanol, neopentanol and 3,3,3-triphenyl-1-propanol occurs with a much slower rate under otherwise identical reaction con-ditions. Such size selectivity suggests that catalysis mainly occurs in the channels. **POST**-1 was also used to catalyze kinetic resolution of *rac*-1-phenyl-2-propanol via transester-ification of **25**. The reaction of **25** with a large excess of *rac*-1-phenyl-2-propanol in the presence of D-**POST**-1 pro-duces the corresponding esters with ~8% enantiomeric ex-cess in favor of *S* enantiomer (Scheme 14). Although mod-est, this is the first observation of an asymmetric induction by modular porous materials.

Lin et al. prepared a series of homochiral porous lamel-lar lanthanide bisphosphonates with a generic formula of [Ln(**L5**-H₂)(**L5**-H₃)(H₂O)₄]·*x*H₂O (Ln: La, Ce, Pr, Nd, Sm, Gd, Tb, *x* = 9–14, **26**–**32**) (Scheme 15) and explored their applications in heterogeneous catalysis and chiral separa-tions [30]. Compounds **26**–**32** were prepared by reacting 2,2′-diethoxy-1,1′-binaphthalene-6,6′-bisphosphonic acid (**L5**-H₄) and lanthanide salts in acidic methanol solutions. The formulation of isostructural **26**–**32** has been confirmed by TGA and microanalysis.

The structure of [Gd(*R*-**L5**-H₂)(*R*-**L5**-H₃)(H₂O)₄]·12H₂O was characterized by single crystal X-ray diffraction (Fig. 24). The 2D lamellar structure contains square anti-prismatic Gd center that have four H₂O molecules and four oxygen atoms of the phosphonate groups of four differ-ent binaphthylbisphosphonates in the coordination sphere. An elongated 2D rhombohedral grid along the *ac* plane is a result of the skewed orientation of the binaphthyl sub-
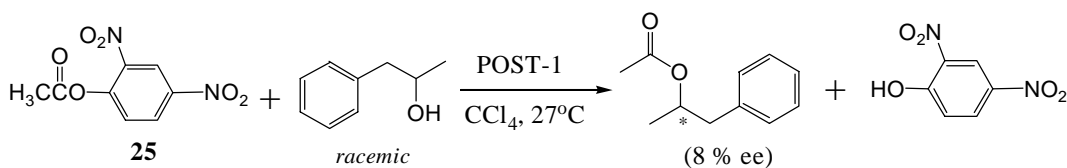
Scheme 14.
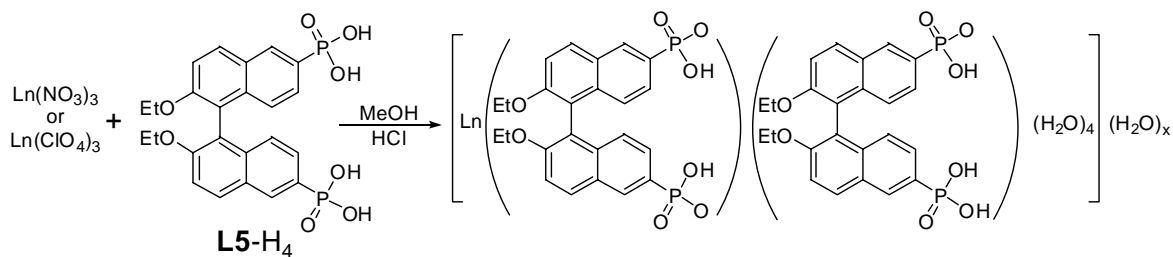
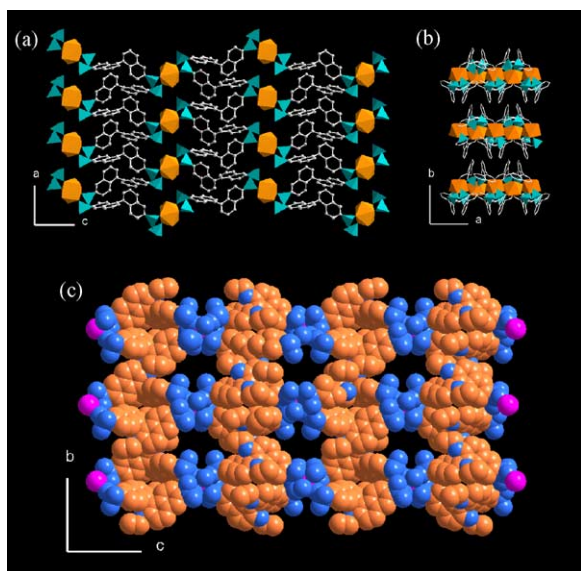Ln = La, Ce, Pr, Nd, Sm, Gd, Tb; x = 9 - 14; **26-32**

Scheme 15.

Fig. 24. 2D structure of [Gd(*R*-**L5**-H$_2$)(*R*-**L5**-H$_3$)(H$_2$O)$_4$]·12H$_2$O: (a) along *a*-axis; (b) showing interdigitation of binaphthyl rings from adjacent layers; (c) space-filling model.

units and the distortion of the tetrahedral phosphonate. The crystal structure reveals interdigitation of the binaphthyl units, however, it is clear from the space filling model that the structure still contains large chiral asymmetric channels with the largest dimension of 12 Å. Removal of water molecules resulted in broadening of the major peaks in the PXRD patterns. However, the original pattern was obtained when the evacuated sample was exposed to water vapor. This suggests that there is a distortion of long-range lamellar type structure whereas the local coordination environment is retained during desolvation. Desolvated structures appear to be ideal candidates to study enantioselective separation and catalysis as they show reversible dehydration and framework stability.

Compound **30** was tested as a chiral Lewis acid catalyst for several organic transformations. Compound **30** is indeed an active catalyst for cyanosilylation of aldehydes. Benzaldehyde, 1-naphthaldehyde, and propionaldehyde reacted with trimethylsilyl cyanide to afford the corresponding cyanohydrin products at 69, 55 and 61% isolated yield, respectively. Varying sizes of the aldehydes did not affect the catalytic activity, suggesting the expansion of the lamellar lanthanide phosphonates to accommodate the substrates. Compound **30** was also shown to be effective in catalyzing ring opening of meso-carboxylic anhydride and Diels-Alder reactions. All these catalytic reactions are believed to be heterogeneous in nature, as the supernatants from the reactions were inactive in catalyzing these reactions. Unfortunately, there is essentially no enantioselectivity for all these reactions. Such a lack of enantioselectivity was a direct consequence of the highly symmetrical coordination environment around the catalytically active Sm centers.

Lin et al. has succeeded in demonstrating the utility of ammonia treated samples of *R*-**30** in chiral separation. Racemic trans-1,2-diaminocyclohexane was separated with *R*-**30** at a substrate/host ratio of 1.4 and an enantio enrichment ratio of 13.6% and 10% for *S,S*-1,2- and *R,R*-1,2-diaminocyclohexane in the beginning and ending fractions, respectively.

In order to improve the enantioselectivity, Lin et al. designed chiral porous Zr phosphonates with pendant 2,2′-bis(diphenylphosphino)-1,1′-binaphthyl (BINAP) groups. Homogeneous Ru and Rh-BINAP complexes are well studied and known to enantioselectively catalyze the reduction of many unsaturated substrates [31]. Lin et al.'s strategy lie in combining the robustness of metal phosphonate frameworks and enantioselectivity of the metal complexes of the pendant chiral chelating bisphosphines to obtain a highly enantioselective heterogeneous catalyst. In order to synthesize these chiral porous solids, two different BINAP derivatives 2,2′-bis(diphenylphosphino)-1,1′-binaphthyl-6,6′-bis (phosphonic acid) (**L13**-H$_4$) and 2,2′-bis(diphenylphosphino)-1,1′-binaphthyl-4,4′-bis(phosphonic acid) (**L14**-H$_4$) were prepared [32]. [Ru(benzene)Cl$_2$]$_2$ was reacted with 1 equivalent of **L13**-H$_4$ and **L14**-H$_4$ in DMF at 100 °C, respectively. The resulting Ru(**L13**-H$_4$)(DMF)$_2$Cl$_2$ and Ru(**L14**-H$_4$)(DMF)$_2$Cl$_2$ were refluxed with Zr(O^{t}Bu)$_4$ in MeOH to give solids formulated as Zr[Ru(**L13**)-DMF)$_2$Cl$_2$]· 2MeOH, (**33**) and Zr[Ru(**L14**)-DMF)$_2$Cl$_2$]·2MeOH (**34**), respectively, based on microanalysis and TGA (Scheme 16).
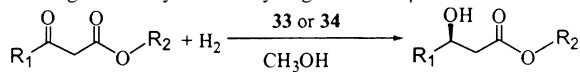
N$_2$ adsorption measurements indicated that **33** and **34** possess high porosity and surface areas. Compound **33** shows a total BET surface area of 475 m^2/g with microporous surface area of 161 m^2/g and a pore volume of 1.02 cm^3/g. For **34**, the total BET surface area is 387 m^2/g with microporous surface area of 154 m^2/g and a pore volume of 0.53 cm^3/g. The solids are amorphous as judged by the PXRD patterns. Both **33** and **34** are very effective heterogeneous catalysts for asymmetric hydrogenation of keto esters. Compound **33** catalyzes hydrogenation of β-keto esters with complete conversion and high e.e.'s ranging from 91.7 to 95.0% (Table 1). The enantio-enrichment of **33** is the same as the parent homogeneous BINAP-Ru catalyst. Direct couple plasma spectroscopy indicated that no leaching of Ru has occurred during the catalytic reactions. The heterogeneous nature of these reactions is confirmed by the lack of catalytic activity of the supernatants of **33** and **34**. Compound **33** was also reused in the asymmetric hydrogenation of methyl acetoacetate for five cycles with complete conversion and no significant deterioration of enantioselectivity.
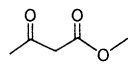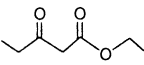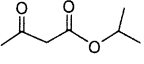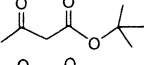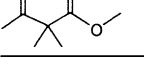
This success has led Lin et al. to design an even more active and enantioselective heterogeneous catalyst. Previously discussed bisphosphine (BINAP) derivatives were treated with [Ru(benzene)Cl$_2$]$_2$ dimer in DMF at 100 °C and diphenylethylenediamine (DPEN). The resulting solid was refluxed with Zr(O^{t}Bu)$_4$ in MeOH to afford the porous chiral solids, Zr[Ru(**L14**-H$_4$)(DPEN)Cl$_2$]·4H$_2$O (**35**) and Zr[Ru(**L13**-H$_4$)(DPEN)Cl$_2$]·4H$_2$O (**36**) (Scheme 17) [33].
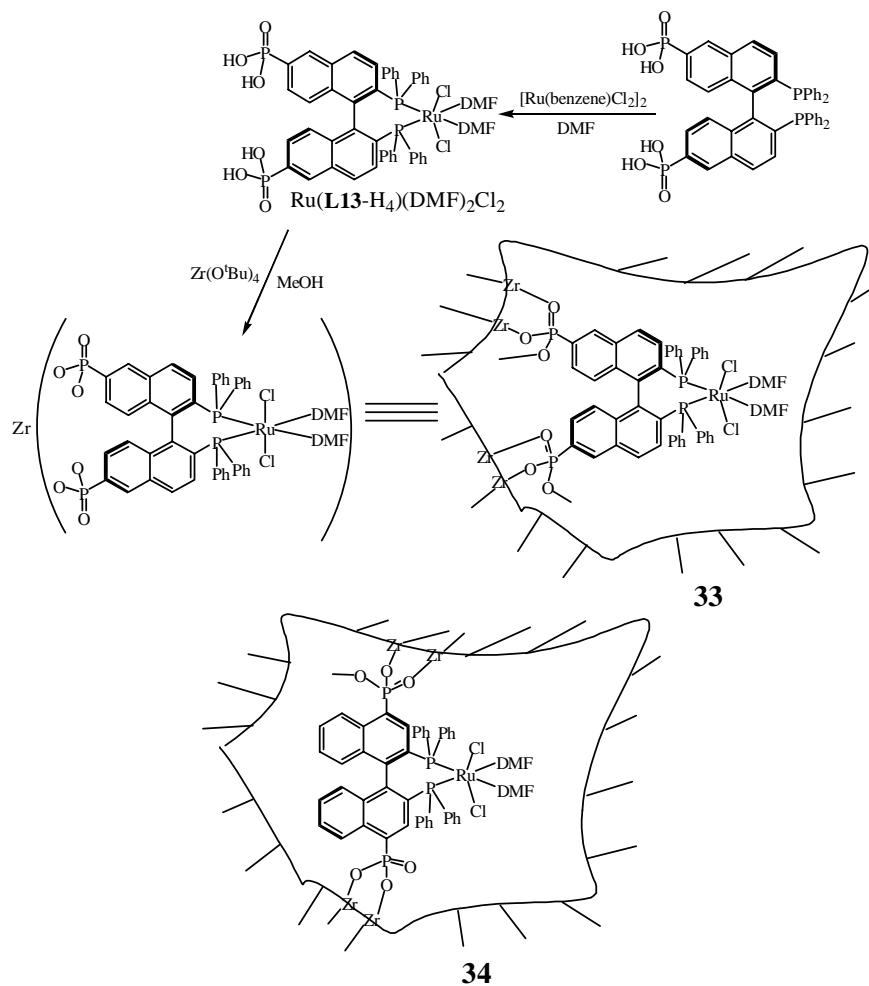
Scheme 16.

Table 1
Heterogeneous asymmetric hydrogenation of β-keto esters

Substrate	Catalyst loading (%)	Temperature	H$_2$ pressure	**33** e.e. (yield)	**34** e.e. (yield)
	1	60 °C	700 (psi)	94.0 (100)	
	1	RT	1400	95.0 (100)	73.1 (90)
	0.1	60 °C	700	93.3 (100)	
	1	RT	1400	92.0 (100)	65.0 (100)
	1	RT	1400	91.7 (100)	68.1 (85)
	1	RT	1400	93.1 (100)	64.0 (100)
	1	RT	1400	93.3 (100)	78.8 (70)
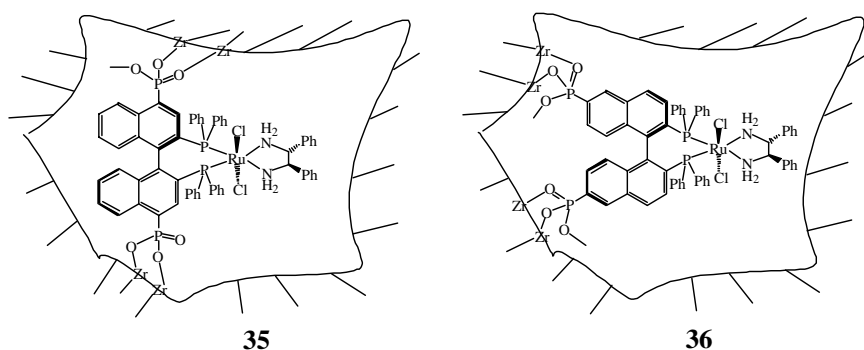
Scheme 17.

The porosity of these amorphous solids was established by N_2 adsorption measurements. For **35**, the total BET surface area is $328\,m^2/g$ with microporous surface area of $60\,m^2/g$ and a pore volume of $0.65\,cm^3/g$, and for **36**, A_{BET} is $400\,m^2/g$ with microporous surface area of $81\,m^2/g$ and a pore volume of $0.98\,cm^3/g$ (Fig. 25). The presence of the DPEN entity on the Zr phosphonate system enhanced the activity and enantioselectivity of hydrogenation of aromatic ketones (Table 2). When 0.1 mol% of **35** in isopropanol was used, acetophenone was hydrogenated to 1-phenylethanol with complete conversion and 96.3% e.e. **36** have a lower e.e. of 79.0%. For comparison, the parent homogeneous Ru-BINAP-DPEN catalyst only exhibits ~80% e.e. for the same reaction. Table 2 lists the series of substrates tested that all show complete conversion and high e.e.'s in the range of 90.6–99.2% for **35**. Lowering the amount of catalyst to 0.02 mol% of solid **35** gave complete conversion and 98.9% e.e. in 20 h. On the other hand, a longer time (40 h) was required for hydrogenation of 1-acetonaphthone with 0.005% catalyst loading but the e.e. remains the same.

The TOF for complete conversion and 70% conversion were calculated to be ~500 and ~$700\,h^{-1}$, respectively.
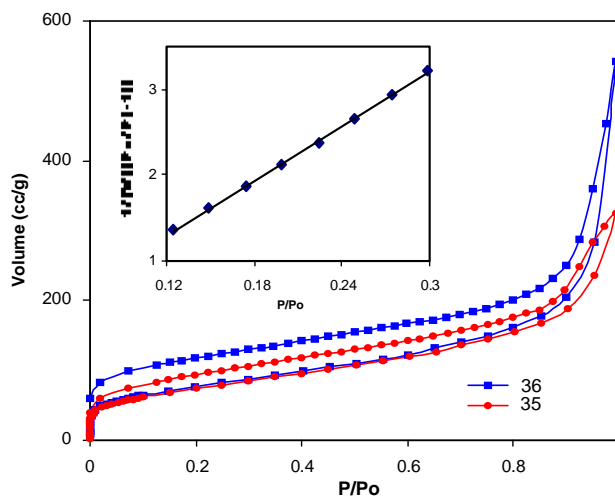
Fig. 25. N_2 adsorption isotherms of **35** and **36**.

35 could be readily recycled and reused for asymmetric hydrogenation of 1-acetonaphthone for up to eight times. These solids thus represent highly active and enantioselective heterogeneous catalysts. The tunability of such a molecular

Table 2
Heterogeneous asymmetric hydrogenation of aromatic ketones
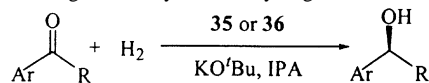
Substrate	Solid loading (%)	KO^{t}Bu	35 e.e. (%)	36 e.e. (%)
Ar: Ph, R: Me	0.1	1	96.3 (97.1)[a]	79.0 (81.3)[a]
Ar: 2-naphthyl, R: Me	0.1	1	97.1	82.1
Ar: 4′-^{t}Bu-Ph, R: Me	0.1	1	99.2	91.5
Ar: 4′-MeO-Ph, R: Me	0.1	1	96.0	79.9
Ar: 4′-Cl-Ph, R: Me	0.1	1	94.9	59.3
Ar: 4′-Me-Ph, R: Me	0.1	1	97.0	79.5
Ar: Ph, R: Et	0.1	1	93.1	83.9
Ar: Ph, R: *cyclo*-Pr	0.1	1	90.6	–
Ar: 1-naphthyl, R: Me	0.1	1	99.2	95.8
	0.02	0.4	98.9	
	0.005	0.02	98.8 (70%)[b]	
	0.005	0.02	98.6[c]	

[a] Homogeneous reactions.

[b] 70% conversion.

[c] 40 h reaction time.

building block approach promises to lead to other practically useful heterogeneous asymmetric catalysts.

5. Concluding remarks and outlook

This paper summarizes the latest developments in the area of homochiral MOCNs in terms of synthesis and characterization, and their applications in enantioselective separation and catalytic processes. Chiral MOCNs of diverse topologies and functionalities can be designed via a modular approach. The facile tunability of such molecular building blocks should allow precise engineering of chiral cavities and functionalities within these chiral porous MOCNs. Practically useful heterogeneous asymmetric catalysts can be envisioned, and highly effective chiral separation media can also be expected. Chiral porous MOCNs thus promise to lead to breakthroughs in chirotechnology.

References

[1] D.W. Breck, Zeolite Molecular Sieves, Structure, Chemistry, and Use, Wiley, New York, 1974.
[2] A. Corma, Chem. Rev. 97 (1997) 2373.
[3] J.M. Newsam, M.M.J. Treacy, W.T. Koetsier, C.B. de Gruyter, Proc. R. Soc. London Ser. A 420 (1988) 375.
[4] M.W. Anderson, O. Terasaki, T. Ohsuna, A. Philippou, S.P. MacKay, A. Ferreira, J. Rocha, S. Lidin, Nature 367 (1994) 347.
[5] C.S. Cundy, P.A. Cox, Chem. Rev. 103 (2003) 663.
[6] (a) P.J. Hagrman, D. Hagrman, J. Zubieta, Angew. Chem. Int. Ed. 38 (1999) 2638;
(b) M. Munakata, L.P. Wu, T. Kuroda-Sowa, Adv. Inorg. Chem. 46 (1999) 173;
(c) M.J. Zaworotko, B. Moulton, Chem. Rev. 101 (2001) 1629;
(d) S.R. Batten, R. Robson, Angew. Chem. Int. Ed. Engl. 37 (1998) 1461;
(e) M. Eddaoudi, D.B. Moler, H. Li, B. Chen, T.M. Reineke, M. O'Keeffe, O.M. Yaghi, Acc. Chem. Res. 34 (2001) 319.
[7] M. Eddaoudi, J. Kim, N. Rosi, D. Vodak, J. Wachter, M. O'Keeffe, O.M. Yaghi, Science 295 (2002) 469.
[8] T. Ezuhara, K. Endo, Y. Aoyama, J. Am. Chem. Soc. 121 (1999) 3279.
[9] C.J. Kepert, T.J. Prior, M.J. Rosseinsky, J. Am. Chem. Soc. 122 (2000) 5158.
[10] A. Jouaiti, M.W. Hosseini, N. Kyritsakas, Chem. Commun. (2002) 1898.
[11] Y. Cui, L.H. Ngo, W. Lin, Chem. Commun. (2003) 1388.
[12] Y. Cui, L.H. Ngo, P.S. White, W. Lin, Inorg. Chem. 42 (2003) 652.
[13] Y. Cui, L.H. Ngo, P.S. White, W. Lin, Chem. Commun. (2003) 994.
[14] O.R. Evans, D.R. Manke, W. Lin, Chem. Mater. 14 (2002) 3866.
[15] J.A. Barron, S. Glazier, S. Bernhard, K. Takada, P.L. Houston, H.D. Abruna, Inorg. Chem. 42 (2003) 1448.
[16] S. Bernhard, K. Takada, D.J. Diaz, H.D. Abruna, H. Murner, J. Am. Chem. Soc. 123 (2001) 10265.
[17] Y. Cui, O.R. Evans, L.H. Ngo, P.S. White, W. Lin, Angew. Chem. Int. Ed. 41 (2002) 1159.
[18] Y.-H. Kiang, G.B. Gardner, S. Lee, Z. Xu, E.B. Lobkovsky, J. Am. Chem. Soc. 121 (1999) 8204.
[19] J.J. Bodwin, V.L. Pecoraro, Inorg. Chem. 39 (2000) 3434.
[20] N.G. Pschirer, D.M. Ciurtin, M.D. Smith, U.H.F. Bunz, H.-G. zur Loye, Angew. Chem. Int. Ed. 41 (2002) 583.
[21] A.L. Spek, PLATON, Version 1.62, University of Utrecht, Utrecht, 1999.
[22] H.L. Ngo, W. Lin, J. Am. Chem. Soc. 124 (2002) 14298.
[23] J.D. Ranford, J.J. Vittal, D. Wu, X. Yang, Angew. Chem. Int. Ed. 37 (1998) 1114.
[24] J.D. Ranford, J.J. Vittal, D. Wu, X. Yang, Angew. Chem. Int. Ed. 38 (1999) 3498.
[25] Y. Cui, L.H. Ngo, P.S. White, W. Lin, Chem. Commun. 124 (2002) 1666.
[26] Y. Cui, S.J. Lee, W. Lin, J. Am. Chem. Soc. 125 (2003) 6014.
[27] M. Fujita, Y.J. Kwon, S. Washizu, K. Ogura, J. Am. Chem. Soc. 116 (1994) 1151.
[28] T. Sawaki, T. Dewa, Y. Aoyama, J. Am. Chem. Soc. 120 (1998) 8539.
[29] J.S. Seo, D. Whang, H. Lee, S.I. Jun, J. Oh, Y.J. Jeon, K. Kimoon, Nature 404 (2000) 982.
[30] O.R. Evans, H.L. Ngo, W. Lin, J. Am. Chem. Soc. 123 (2001) 10395.
[31] (a) R. Noyori, Angew. Chem. Int. Ed. 41 (2002) 2008 (and references therein);
(b) R. Noyori, H. Takaya, Acc. Chem. Res. 23 (1990) 345;
(c) M. Kitamura, T. Ohkuma, S. Inoue, N. Sayo, H. Kumobayashi, S. Akutagawa, T. Ohta, H. Takaya, R. Noyori, J. Am. Chem. Soc. 110 (1988) 629.
[32] A. Hu, H.L. Ngo, W. Lin, Angew. Chem. Int. Ed., in press.
[33] A. Hu, H.L. Ngo, W. Lin, J. Am. Chem. Soc. 125 (2003) 11490.